AEDC-TR-78-20

Cy.2

SUPPRESSION OF PERFORATED WALL NOISE IN A TRANSONIC WIND TUNNEL AND THE EFFECTS ON AERODYNAMIC DATA

J. L. Jacocks and R. L. Parker, Jr.
ARO, Inc., a Sverdrup Corporation Company

PROPULSION WIND TUNNEL FACILITY
ARNOLD ENGINEERING DEVELOPMENT CENTER
AIR FORCE SYSTEMS COMMAND
ARNOLD AIR FORCE STATION, TENNESSEE 37389

May 1978

Final Report for Period 1 October 1976 - 30 September 1977

Approved for public release; distribution unlimited.

Prepared for

ARNOLD ENGINEERING DEVELOPMENT CENTER/DOTR
ARNOLD AIR FORCE STATION, TENNESSEE 37389

NOTICES
When U. S. Government drawings, specifications, or other data are used for any purpose other than a definitely related Government procurement operation, the Government thereby incurs no responsibility nor any obligation whatsoever, and the fact that the Government may have formulated, furnished, or in any way supplied the said drawings, specifications, or other data, is not to be regarded by implication or otherwise, or in any manner licensing the holder or any other person or corporation, or conveying any rights or permission to manufacture, use, or sell any patented invention that may in any way be related thereto.
Qualified users may obtain copies of this report from the Defense Documentation Center.
References to named commerical products in this report are not to be considered in any sense as an indorsement of the product by the United States Air Force or the Government.

This report has been reviewed by the Information Office (OI) and is releasable to the National Technical Information Service (NTIS). At NTIS, it will be available to the general public, including foreign nations.

APPROVAL STATEMENT

This report has been reviewed and approved.

Stephen L. Lamkin

STEPHEN L. LAMKIN, Captain, USAF
Project Manager, Research Division
Directorate of Test Engineering

Approved for publication:

FOR THE COMMANDER

Marion L. Laster

MARION L. LASTER
Director of Test Engineering
Deputy for Operations

REPORT DOCUMENTATION PAGE		READ INSTRUCTIONS BEFORE COMPLETING FORM
1 REPORT NUMBER AEDC-TR-78-20	2 GOVT ACCESSION NO.	3 RECIPIENT'S CATALOG NUMBER
4 TITLE (and Subtitle) SUPPRESSION OF PERFORATED WALL NOISE IN A TRANSONIC WIND TUNNEL AND THE EFFECTS ON AERODYNAMIC DATA		5 TYPE OF REPORT & PERIOD COVERED Final Report - 1 October 1976 - 30 September 1977 6 PERFORMING ORG. REPORT NUMBER
7 AUTHOR(s) J. L. Jacocks and R. L. Parker, Jr., ARO, Inc.		8 CONTRACT OR GRANT NUMBER(s)
9 PERFORMING ORGANIZATION NAME AND ADDRESS Arnold Engineering Development Center Air Force Systems Command Arnold Air Force Station, Tennessee 37389		10 PROGRAM ELEMENT, PROJECT, TASK AREA & WORK UNIT NUMBERS Program Element 65807F
11 CONTROLLING OFFICE NAME AND ADDRESS Arnold Engineering Development Center/DOS Air Force Systems Command Arnold Air Force Station, Tennessee 37389		12. REPORT DATE May 1978 13 NUMBER OF PAGES 48
14 MONITORING AGENCY NAME & ADDRESS(if different from Controlling Office)		15 SECURITY CLASS. (of this report) UNCLASSIFIED 15a DECLASSIFICATION/DOWNGRADING SCHEDULE N/A

16 DISTRIBUTION STATEMENT (of this Report)

Approved for public release; distribution unlimited.

17 DISTRIBUTION STATEMENT (of the abstract entered in Block 20, if different from Report)

18 SUPPLEMENTARY NOTES

Available in DDC.

19 KEY WORDS (Continue on reverse side if necessary and identify by block number)

flow
noise reduction
noise suppressors
flow quality
wind tunnel calibration
interference
transonic wind tunnels
walls

20 ABSTRACT (Continue on reverse side if necessary and identify by block number)

Tests were conducted in the AEDC Aerodynamic Wind Tunnel (4T) of the Propulsion Wind Tunnel Facility to determine the effect of screen overlays installed on the airside test section walls for the purpose of suppressing the wall noise. Data are presented to illustrate that the screens and resulting noise reduction affected the test section longitudinal flow uniformity, plenum-stream calibration, wave cancellation properties of the walls, transition

DD FORM 1 JAN 73 1473 EDITION OF 1 NOV 65 IS OBSOLETE

20. ABSTRACT (Continued)

Reynolds number, and shock/boundary-layer interaction. In general, the effect of noise reduction on viscous phenomena was similar to that observed with decreased Reynolds number.

AFSC
Arnold AFS Tenn

PREFACE

The work reported herein was conducted by the Arnold Engineering Development Center (AEDC), Air Force Systems Command (AFSC), for the Directorate of Test Engineering Research, AEDC, under Program Element 65807F. The results were obtained by ARO, Inc., AEDC Division (a Sverdrup Corporation Company), operating contractor for the AEDC, AFSC, Arnold Air Force Station, Tennessee, under ARO Project Numbers P32A-J5A and P32A-J9A. The Air Force project monitor was Capt. S. L. Lamkin. The manuscript was submitted for publication on February 27, 1978.

CONTENTS

ILLUSTRATIONS

Figure

Figure Page

APPENDIX

1.0 INTRODUCTION

Perforated walls in transonic wind tunnels generate noise, termed edgetones, that is thought to degrade the quality of model test data. Methods of suppressing these edgetones are available (Refs. 1 and 2), but no definitive information exists concerning the impact of wall modification on test data. To provide a comprehensive evaluation of the effects of wall modification on tunnel performance parameters and model data, a series of tests was conducted in the AEDC Aerodynamic Wind Tunnel (4T) of the Propulsion Wind Tunnel Facility (PWT).

Edgetone suppression was achieved by using wire screen overlays on the airside of the test section walls. The test program included evaluation of the effects of the wire screen overlay on the Tunnel 4T longitudinal flow uniformity, plenum-stream calibration, and wall crossflow and wave cancellation characteristics. An investigation was also made of the effects of perforated wall edgetone noise on transition Reynolds number and representative static pressure distributions on a test model. The results of the test program and evaluations of the wall characteristics of the modified wall are presented herein.

2.0 APPARATUS

2.1 TUNNEL 4T

The Aerodynamic Wind Tunnel (4T) is a closed-loop, continuous flow, variable density tunnel in which the Mach number can be varied from 0.1 to 1.3 and also can be set at 1.6 and 2.0 by placing nozzle inserts over the permanent nozzle. At all Mach numbers, the stagnation pressure can be varied from 300 to 3,700 psfa. The test section is 4 ft square and 12.5 ft long with perforated, variable porosity (0.5- to 10-percent open) walls. It is completely enclosed in a plenum chamber from which the air can be evacuated, allowing part of the tunnel airflow to be removed through the perforated walls of the test section.

2.2 SCREEN OVERLAY

Preliminary tests conducted in the AEDC Aerodynamic Wind Tunnel (1T) and the AEDC Acoustic Research Tunnel (ART) utilized wire screen overlays of 40 by 60 mesh with wire diameter of 0.006 in. Simple scaling resulted in the selection of 10-mesh screen with 0.020-in.-diam wire for use in Tunnel 4T. Although the screens survived the test, including several removals and re-installations, some physical degradation occurred.

$$\text{porosity} = (1 - md)^2 = (1 - (60)(.006))^2 = .49 \leftarrow 40 \times 60 \times .006$$

$$= (1 - 10(.020))^2 = (1 - .2)^2 = .64 \leftarrow 10 \times 10 \times .020$$

2.3 CALIBRATION MODELS

A static pipe of 2.875-in. diameter was used to determine the centerline Mach number distributions. The pipe was supported at its upstream end by forward-swept struts attached to the nozzle sidewalls and at its downstream end by the half-sector model support. The pipe contained static pressure orifices with nominally 2-in. spacing within the test region.

Wave cancellation properties of the walls were determined utilizing two bodies of revolution of 1-percent blockage. The model geometries consisted of a common cylindrical afterbody with interchangeable forebodies: a 2:1 ellipsoid and a 20-deg included angle cone. Pertinent dimensions of the models are given in Fig. 1 with additional details, such as pressure orifice locations, available in Ref. 3. The cone-cylinder nosetip was located at tunnel station 76 and the ellipse at station 83.

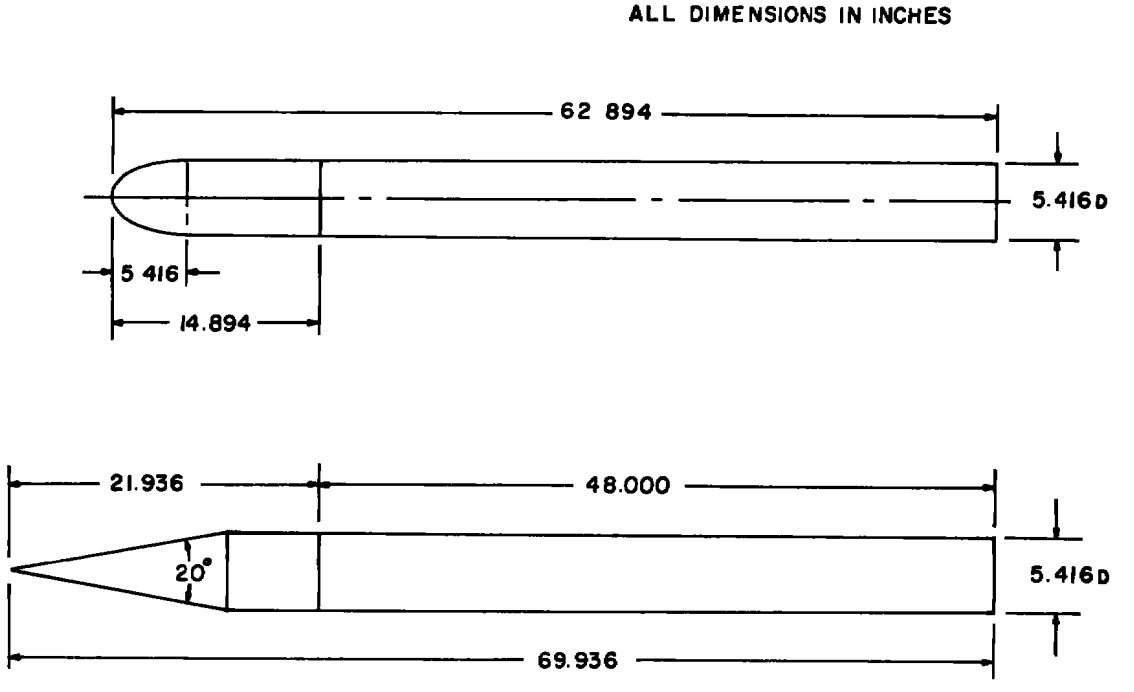

Figure 1. Dimensions of the axisymmetric pressure models.

2.4 TRANSITION CONE

The transition cone model, Fig. 2, is a pointed, stainless steel, 10-deg included angle cone with a surface finish polished to 8- to 12-μin. root-mean-square waviness. The cone is equipped with a traversing pitot probe for transition detection, two surface-mounted 0.25-in.-diam condenser microphones, and a surface temperature thermocouple. The

traversing probe, which traverses along the cone surface at a height of nominally 0.005 in., is equipped with a 0.125-in.-diam strain-gage-type pressure transducer close-coupled to the sensing tube. The cone was installed on the tunnel centerline at zero incidence angle. A more detailed description of the transition cone can be found in Ref. 4.

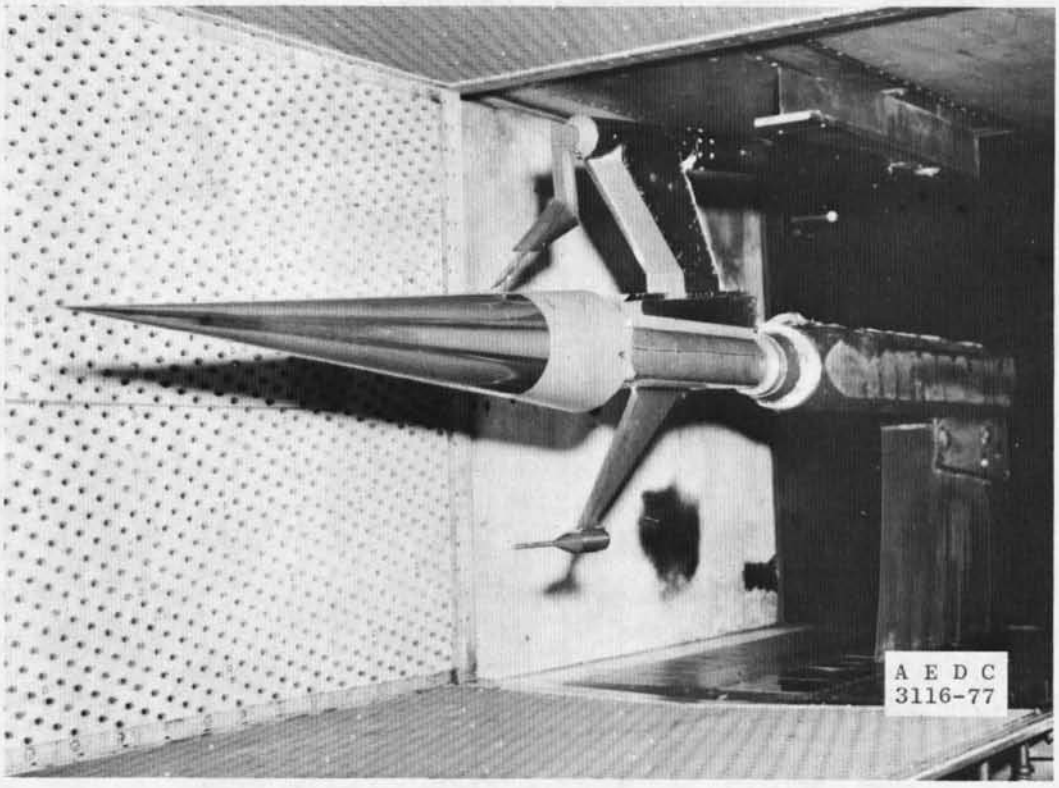

Figure 2. The AEDC transition cone.

2.5 LIFTING MODELS

The lifting models consisted of sting-mounted, wing-body combinations. The geometrically similar models have rectangular planform wings with NACA 63A006 airfoil sections. Pertinent dimensions of the models are given in Fig. 3. The wing models have a longitudinal ray of pressure orifices along the top and bottom of the center bodies and a chordwise ray of pressure orifices at the mid-semispan of the upper right and lower left wing surfaces. The sting supporting the large model was equipped with strain gages to monitor deflections, whereas the small model sting was not instrumented, and its deflections were assumed to be zero.

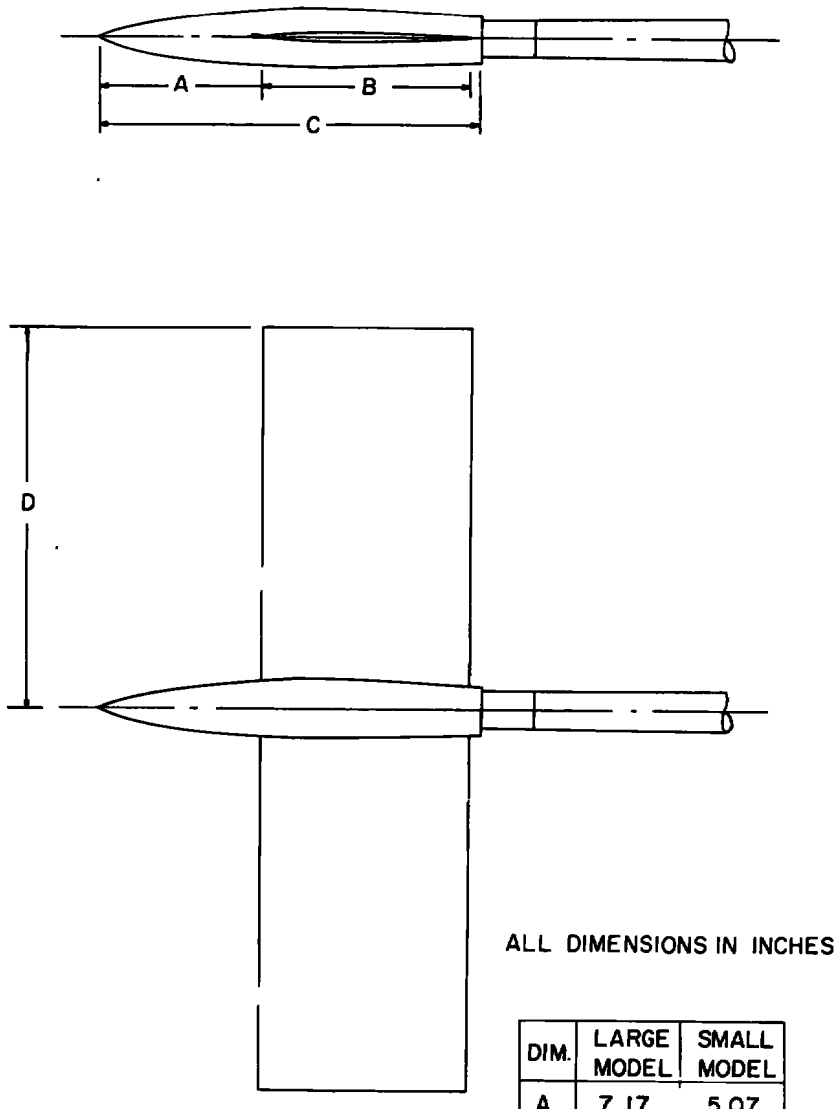

DIM.	LARGE MODEL	SMALL MODEL
A	7.17	5 07
B	9.00	4 50
C	16.50	10.00
D	32.00	13.00

Figure 3. Dimensions of the lifting models.

2.6 INSTRUMENTATION

The static pressure on the model and test section wall was measured with 50 Kistler® transducers referenced to plenum pressure, P_c, and spanned for ±2,160 psf, full scale. Two-position valves associated with each transducer allowed sensing of pressures at up to 100 locations. Primary tunnel parameters (P_c, P_E, and P_T) were measured with Datametric® systems.

3.0 PROCEDURE

3.1 TEST PROCEDURE

Each calibration model and the static pipe were aligned with their centerlines coincident with the tunnel centerline. The test variables were tunnel stagnation pressure, Mach number, and wall porosity, and data were obtained at the following conditions:

$$P_T = 2{,}000 \text{ psfa}$$

$$0.2 \leq M \leq 1.3$$

$$0.5 \leq \tau \leq 7.0 \text{ percent}$$

Limited data were acquired at P_T = 1,200 and 2,500 psfa. The test section Mach number is defined by the plenum-stream calibration, Refs. 5 and 6, for the "screen off" wall configuration and as discussed in Appendix A of this report for the "screen on" configuration. Each of the test variables was set and maintained by automatic computer control, with the exception of Mach number at supersonic test conditions, which was manually controlled.

Manual initiation of the data acquisition cycle resulted in the isolation (trapping) of the transducer reference pressure with subsequent computer scanning of each transducer readout until steady-state readings were indicated. The transducer valves were then switched on computer command, and another pressure-lag routine was executed; then the trapped reference was released. Tunnel conditions were computed on the basis of the average of the two data acquisition periods.

Data were obtained with the transition cone at unit Reynolds numbers of 2, 3, and 4 x 10^6 per foot. The cone was aligned with the geometric centerline of the wind tunnel, and the incidence to the test section flow was assumed to be zero. Location of the transition point was obtained by traversing the pitot probe in the forward direction in all cases while holding tunnel conditions as constant as possible. Sufficient time was allowed for the cone temperature to reach equilibrium with the flow to minimize heat-transfer effects.

Data were obtained with the lifting models at Mach numbers of 0.60, 0.80, 0.90, and 0.95. The unit Reynolds number was varied from 1.5 to 4.8 x 10^6 per foot by adjusting stagnation pressure, which along with the two wing chord lengths of 4.5 and 9 in., provided a chord Reynolds number variation from nominally 0.6 to 3.6 x 10^6. Data were obtained at the above conditions both with natural boundary-layer transition on the

wing surfaces and with an artificial trip consisting of distributed No. 90 glass beads at the 5-percent chord location. To permit comparison of the wing pressure distributions between the various model and tunnel configurations at a constant angle of attack, the model gravimetric angle of attack was matched at discrete values within ±0.05 deg and was defined as

$$\alpha = \alpha_i + \Delta\alpha$$

where

α = gravimetric angle of attack

α_i = sting support angle

and

$\Delta\alpha$ = sting deflection angle (assumed to be zero for the small model).

3.2 PRECISION OF MEASUREMENTS

Uncertainties (95-percent confidence level) in the instrumentation systems were estimated from repeated calibrations of the systems against secondary standards whose precisions are traceable to the National Bureau of Standards. These uncertainties were combined using the Taylor series method of error propagation to determine the precision of the reduced parameters, which are shown below.

Parameter	Uncertainty (±)
ΔM	0.0055
ΔM_l	0.0035
ΔM_c	0.0033
ΔDM	0.0035
$\Delta P/P_T$	0.0034
$\Delta\lambda$	0.0043
$\Delta\tau$	0.07
$\Delta 2\sigma$	0.0012
ΔC_p	0.010
$\Delta\alpha$	0.10

4.0 RESULTS AND DISCUSSION

4.1 LONGITUDINAL FLOW UNIFORMITY

Representative centerline Mach number distributions are presented in Fig. 4 at wall porosities of three and five percent. For the subsonic Mach numbers, plenum suction was achieved via reentry diffuser flaps at the exit of the test section on the basis of the results of Ref. 5. This mode of operation, rather than using auxiliary suction, resulted in excessive tunnel pressure ratio with corresponding Mach number gradients at the downstream end of the test section. Since subsequent tests with the screens would not be affected by these gradients, tunnel operation procedure was not altered.

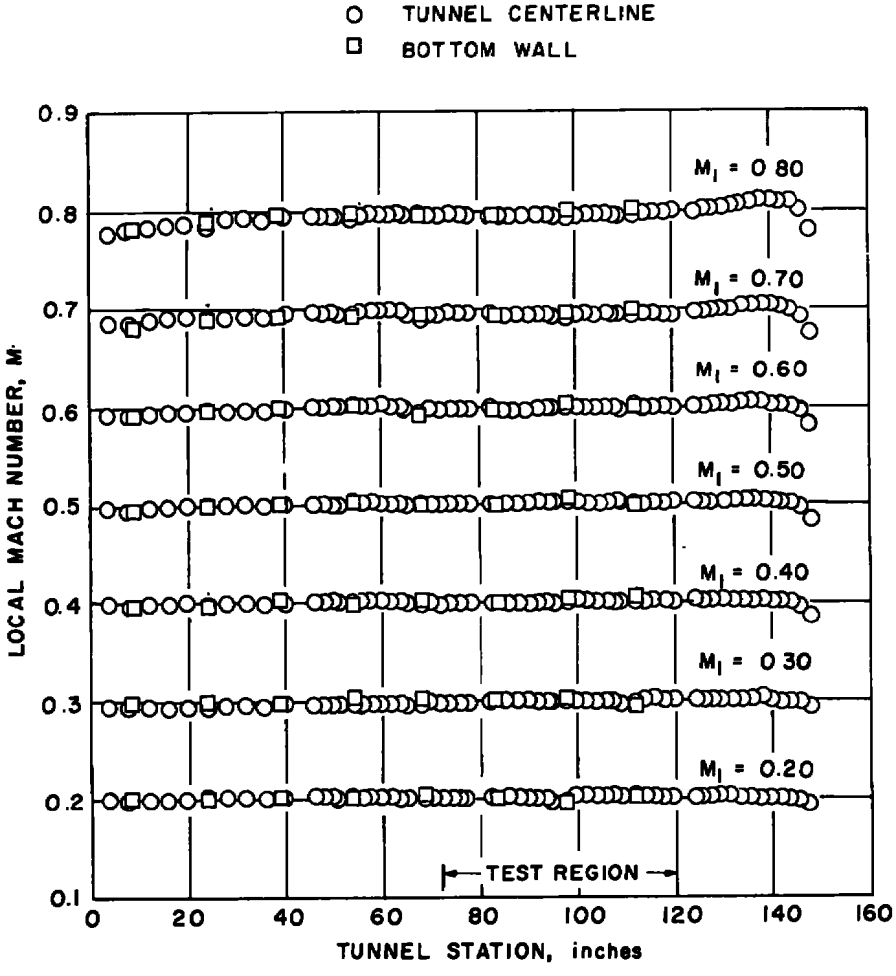

a. $\tau = 3$, $0.20 < M_1 < 0.80$

Figure 4. Tunnel centerline and bottom wall Mach number distribution.

Also given in Fig. 4 is the Mach number distribution as indicated by static pressure measurements on the bottom wall. The orifices were installed in the studs which support the airside wall. Since the studs were not uniformly flush, there are individual bias errors associated with each orifice. Nonetheless, reasonable consistency of the wall and centerline data is evident, and the wall static pressure can provide an independent estimate of the test section Mach number and longitudinal flow uniformity.

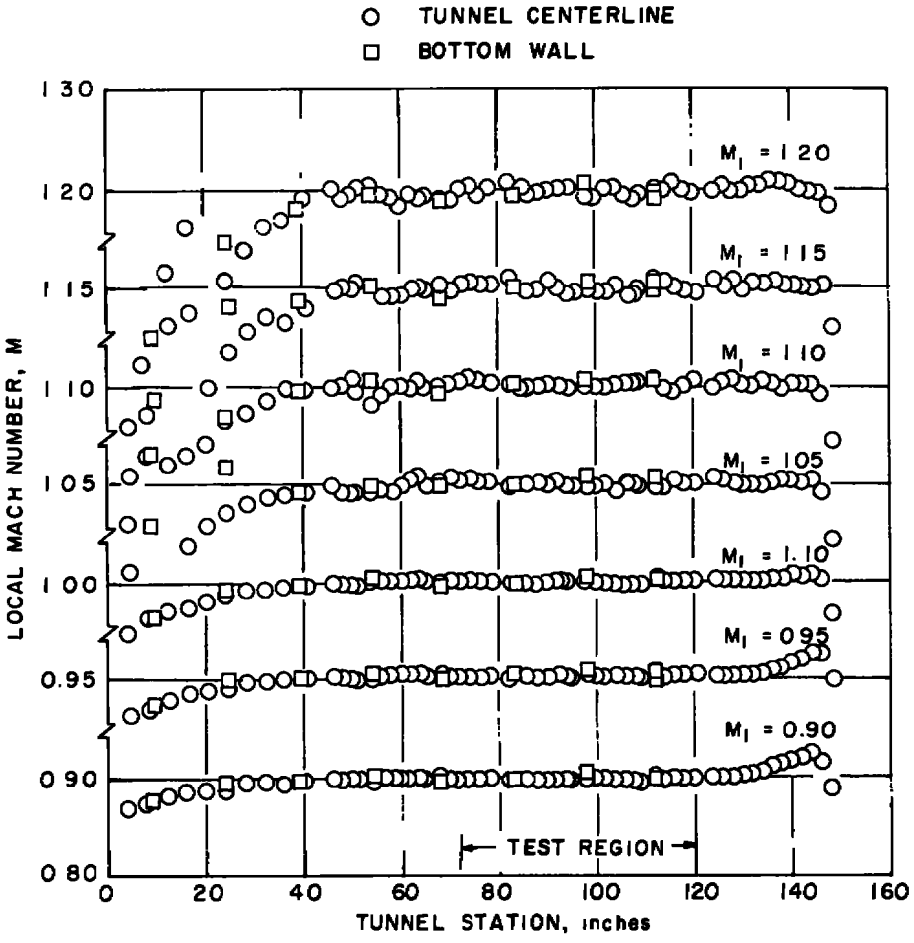

b. τ = 3, 0.90 < M_1 < 1.20

Figure 4. Continued.

A quantitative description of the degree of flow uniformity is provided by the standard deviation of the Mach number distribution. These results are given in Fig. 5 along with comparative data from Refs. 5 and 6, which are the basic tunnel (screen off) calibrations. Also given in Fig. 5 are the upper limits of acceptable Mach number deviation as defined in Ref. 7, which are exceeded at five-percent porosity for Mach numbers of 1.15 and 1.20 with the screens installed. In general, the screens had an adverse effect on the flow uniformity, but flow of good quality was nonetheless obtainable, particularly at reduced wall porosity. (It should be noted that the test region was defined as extending from tunnel station 72 to 120 with the screens installed, whereas the normal test region is from station 72 to 140.) A portion of the degradation

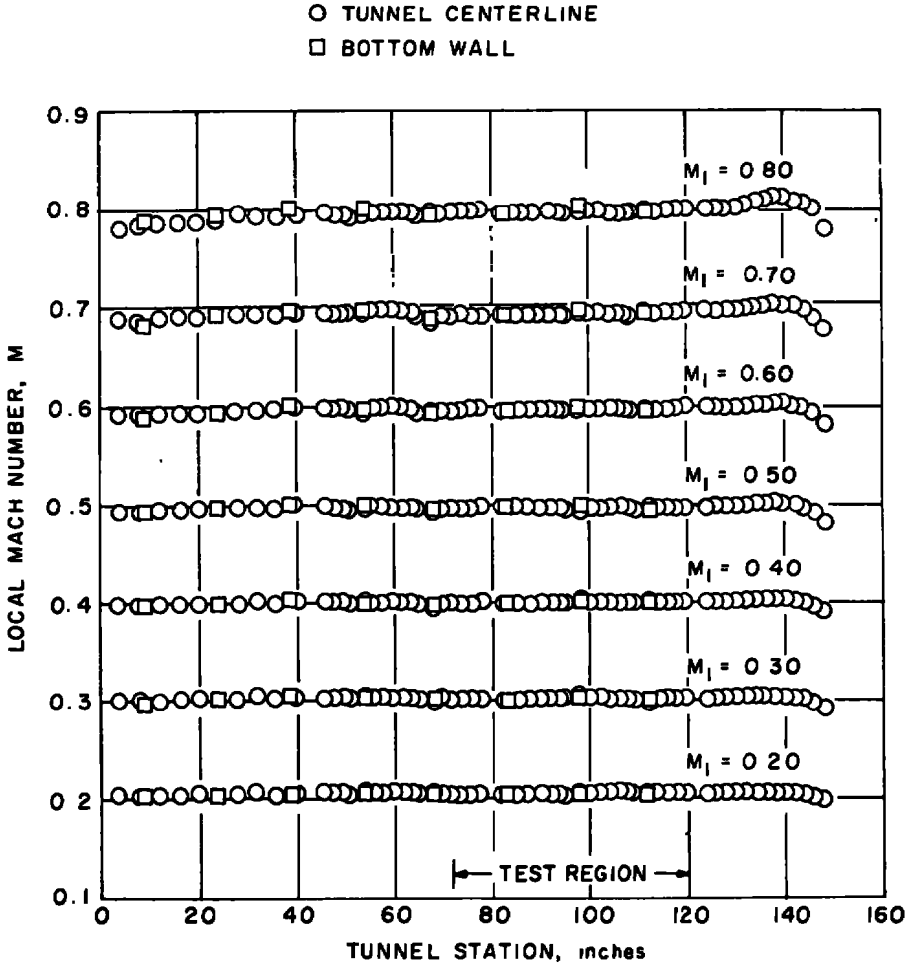

c. $\tau = 5$, $0.20 < M_1 < 0.80$

Figure 4. Continued.

in flow quality may be attributed to the method selected for the screen installation. The screen was attached to the walls with round-head screws and washers which were exposed to the airstream and thus introduced disturbances into the flow.

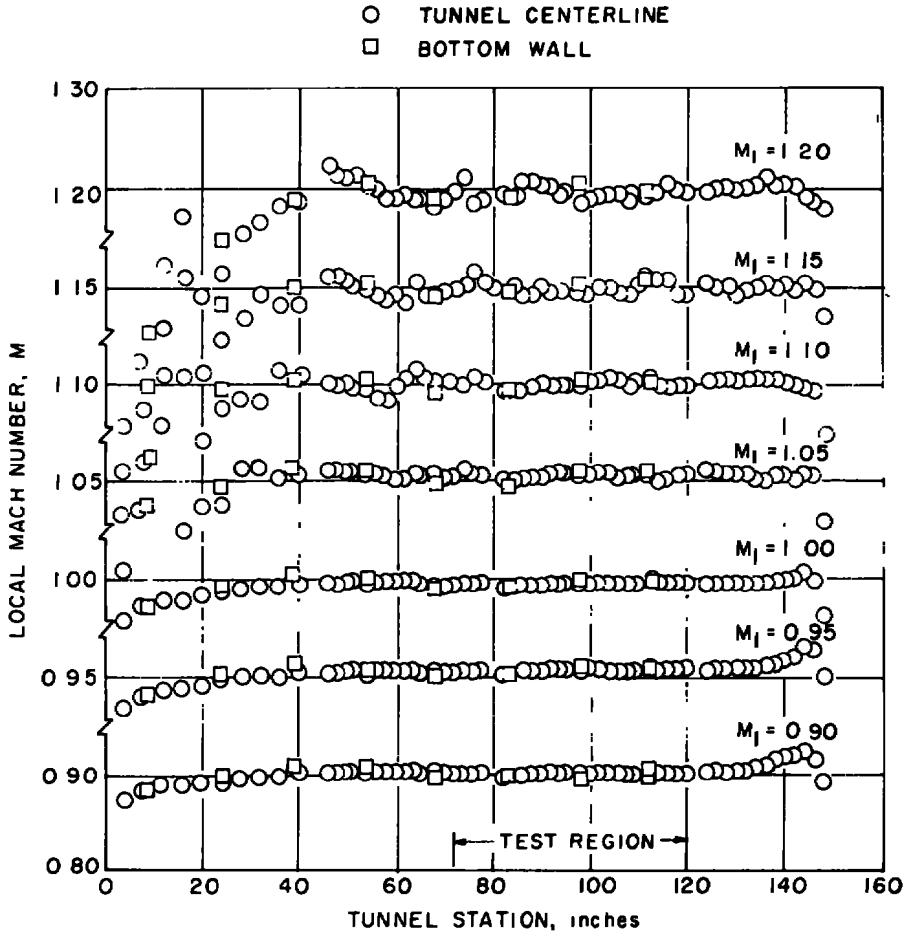

d. τ = 5, 0.90 < M_1 < 1.20
Figure 4. Concluded.

A second source of disturbances with the screen installed was a wedge plate of 0.125-in. thickness installed at tunnel station 1.0 on each wall for the purpose of fastening the screen leading edge to the wall. These plates formed an effective nozzle throat and generated overexpansions in the flow at supersonic Mach numbers. As illustrated in Fig. 6, the subsequent local flow disturbance was multiply reflected from the tunnel walls (at τ = 5 percent) and was the major contribution to the degradation in flow quality at supersonic Mach numbers.

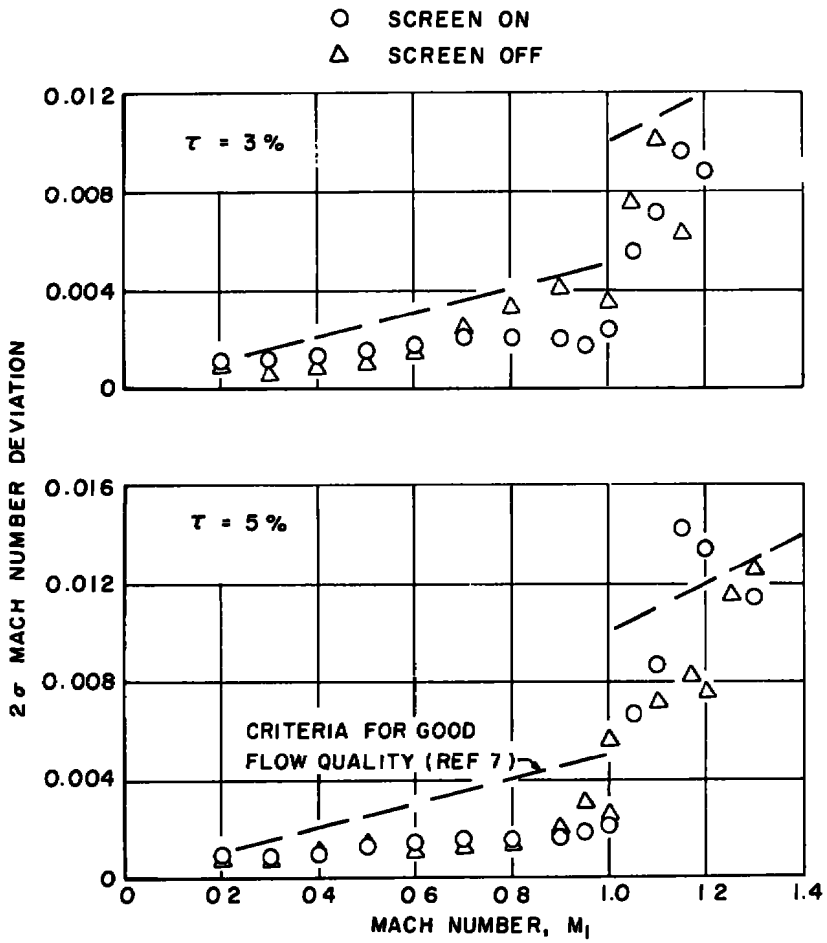

Figure 5. Comparison of the longitudinal flow uniformity with and without the wall screens.

4.2 WAVE CANCELLATION

The primary function of a variable porosity test section wall is to minimize model-generated shock and expansion waves reflecting from the wall and impinging back on the model. The porosity required for the cancellation of these waves is a monotonic function of Mach number, increasing from 1.5 percent at M = 1.0 to 6.2 percent at M = 1.3, for the screen-off wall configuration. The common method of assessing the quality of wave cancellation is the examination of pressure distributions on bodies of revolution and comparison with pressure distributions for the same body geometry in an interference-free environment. Two models were used for this purpose, a 20-deg included angle cone-cylinder and a 2:1 ellipsoid-cylinder as previously described.

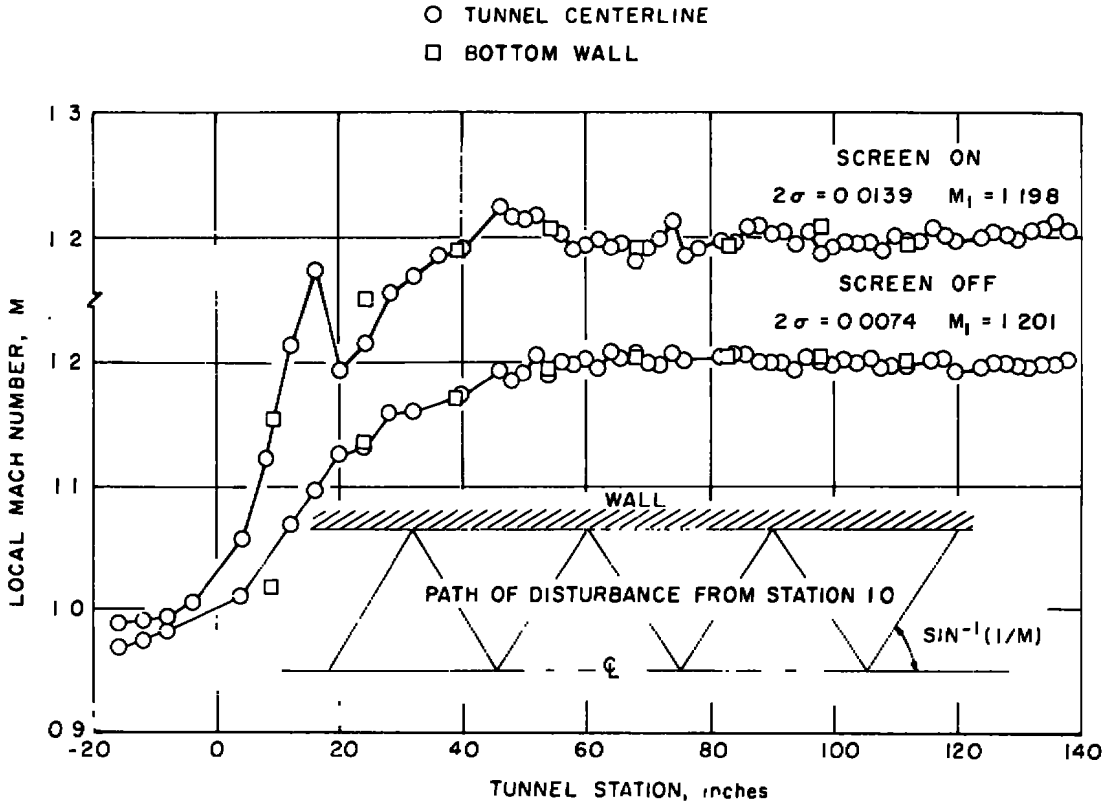

Figure 6. Comparison of the Mach number distribution with and without the wall screens.

4.2.1 Cone-Cylinder Model

Pressure distributions on the cone-cylinder model are presented in Fig. 7 and compared with screen-off results from Ref. 8 and the interference-free data of Ref. 3. At a given geometric wall porosity, the screen changed the wall crossflow properties to yield an "effective" increase in open area. Thus, cancellation of the model compression waves with the screen installed occurred either at increased Mach number for fixed porosity or at decreased porosity for a given Mach number relative to screen-off conditions.

The effect of porosity changes at a fixed Mach number of 1.1 is illustrated in Fig. 8. Although there is an attached bow shock, the cone surface flow is subsonic. Wall porosity changes with the screens produce significant variations in the cone pressure distributions relative to the results obtained without screens (Ref. 8). Progressive deviation of the cone pressure distribution from the interference-free results occurred with reduction of wall porosity, yet low wall porosity is required for wave cancellation at this Mach number. Comparison of the data taken at 2.0 and 2.5 percent porosity with screens indicates that

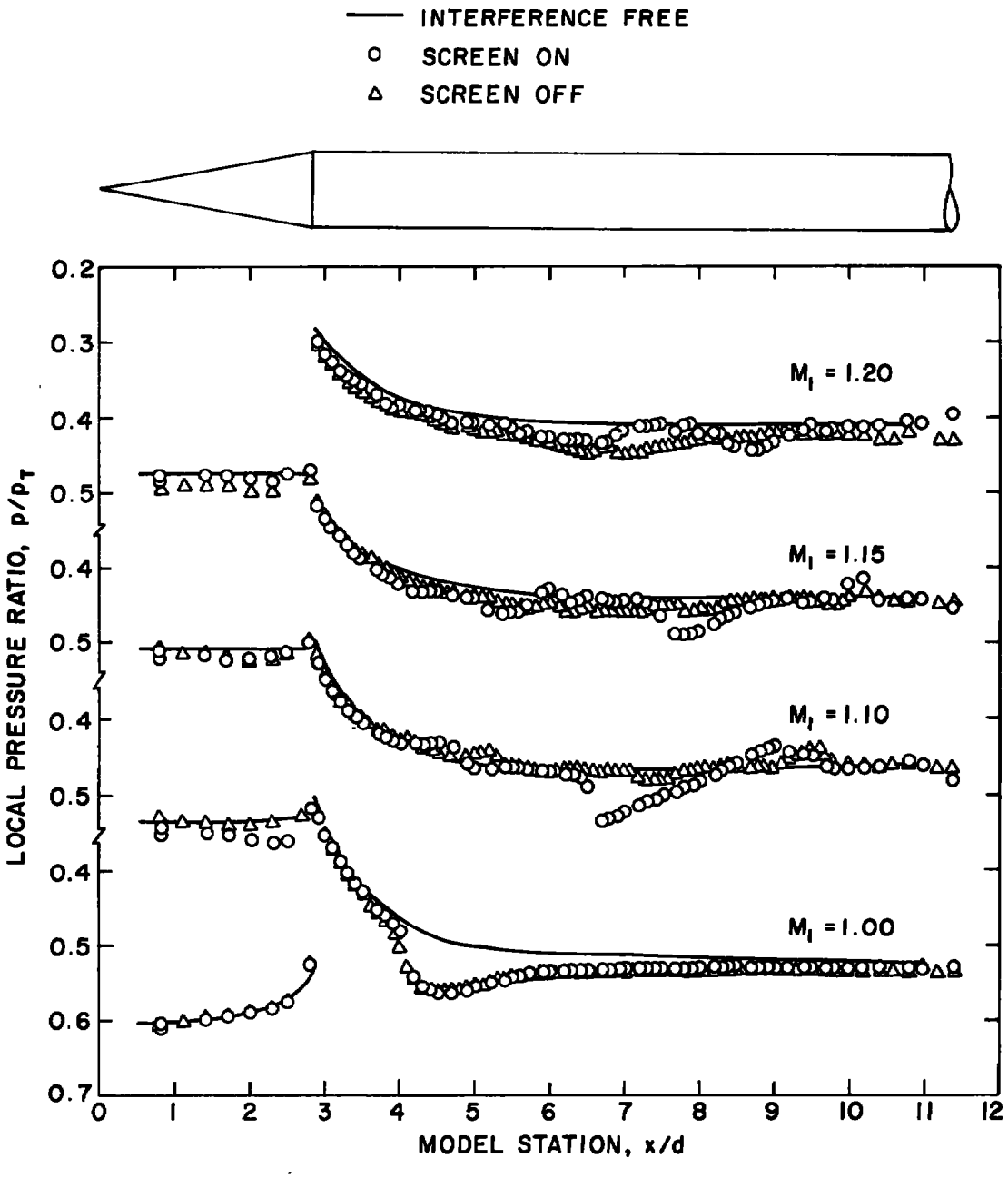

a. τ = 3.0 percent

Figure 7. Pressure distribution on the 20-deg cone-cylinder model, τ = 3 percent.

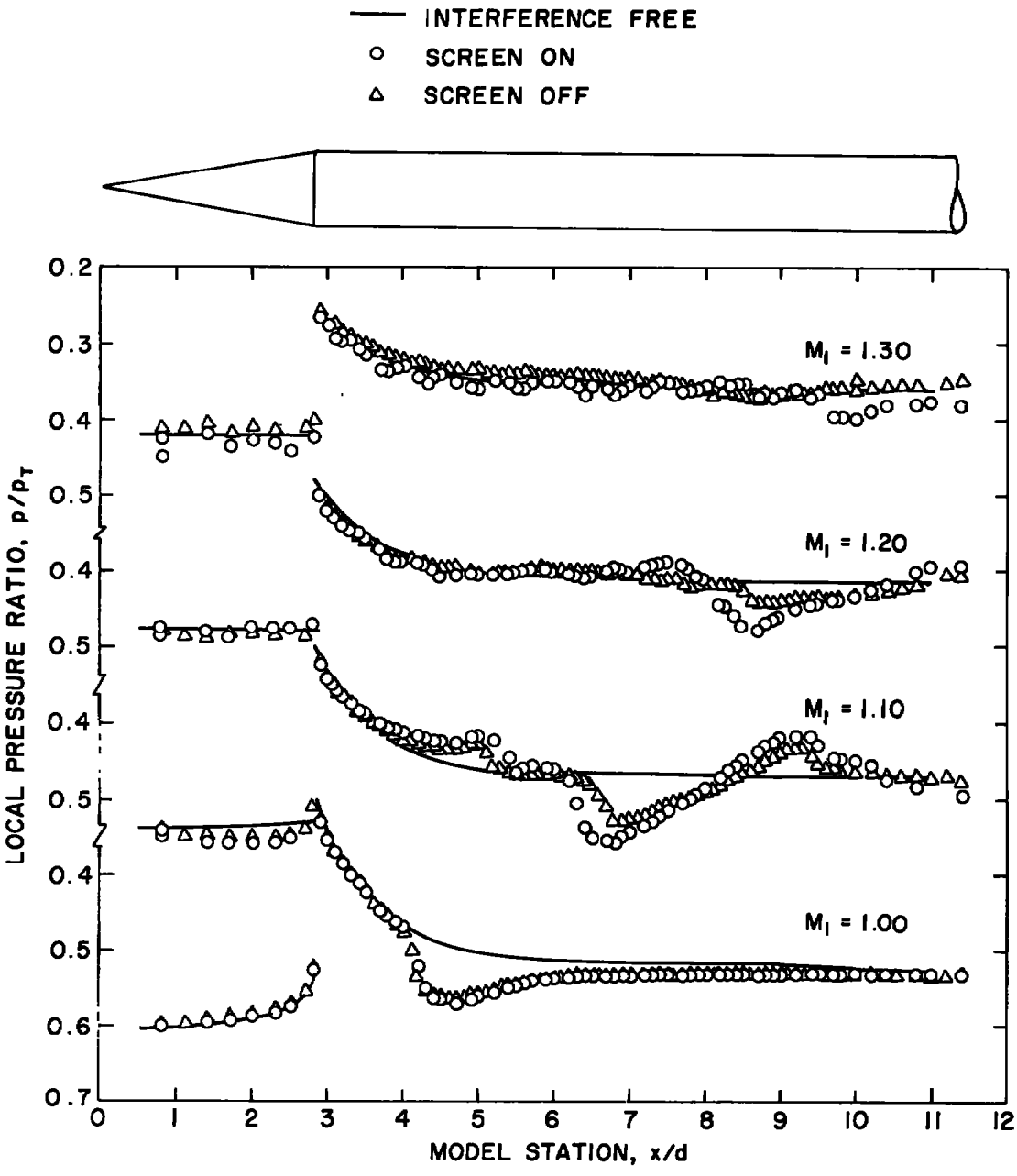

b. τ = 6.0 percent
Figure 7. Concluded.

the best porosity for compression-wave cancellation lies somewhere between these porosities. The demarcation between compression and expansion waves impinging on the wall and reflecting back to the model occurs at x/d = 6.5, and the nonuniformity downstream of this station indicates that a porosity of something less than 2.0 percent would be required for optimum expansion wave cancellation with screens at M = 1.1.

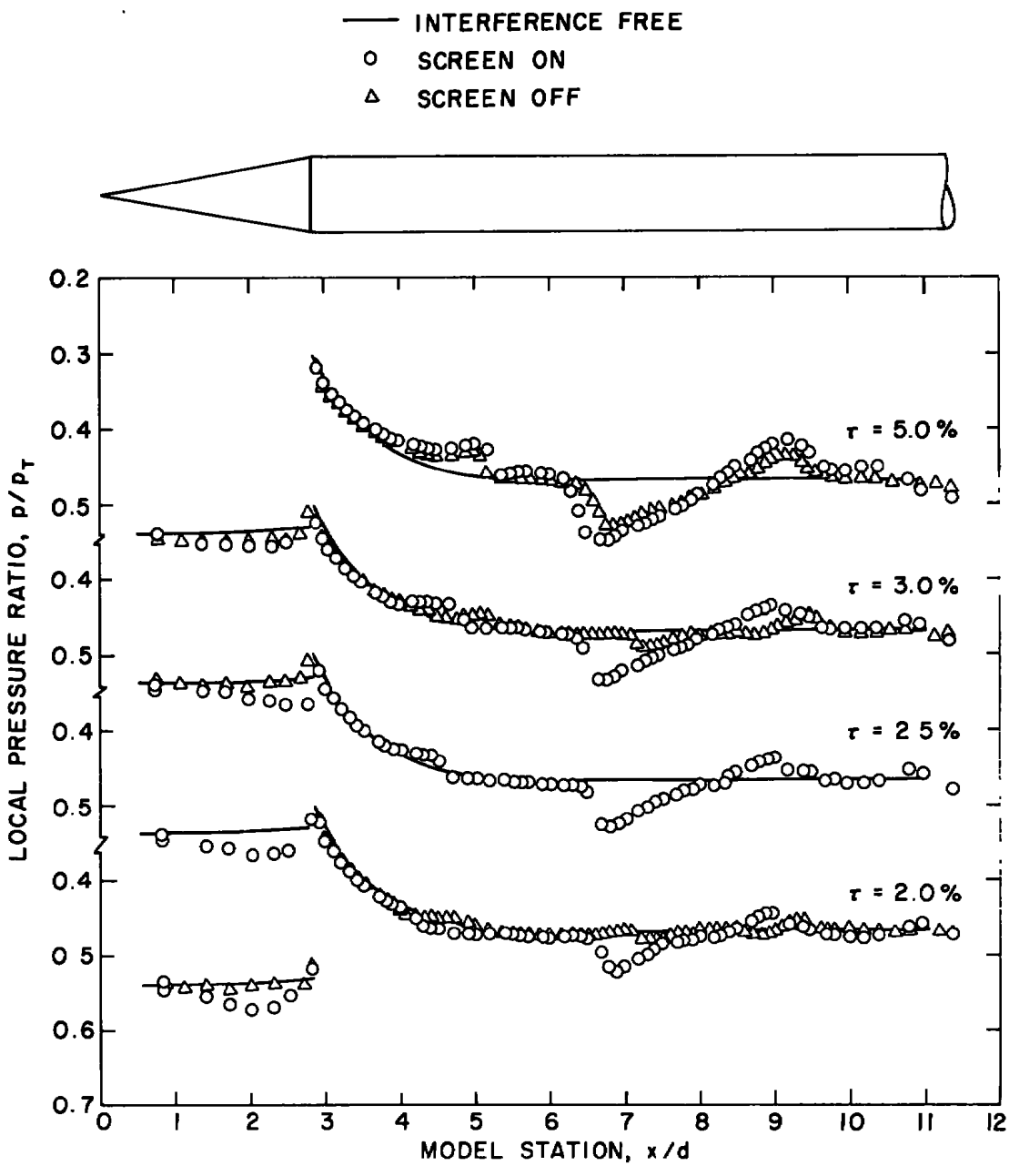

Figure 8. Pressure distribution on the 20-deg cone-cylinder model for various porosities at M_1 = 1.10.

4.2.2 Ellipse-Cylinder Model

Representative pressure distributions obtained with the elliptic nose are presented in Figs. 9 and 10 with the interference-free results derived from the computations of Ref. 9 (Hsieh) and Ref. 3. The degradation of the wave cancellation properties of the wall with

the screen is not demonstrated clearly by these results. However, it is clear that the screen changed the model/tunnel flow interaction.

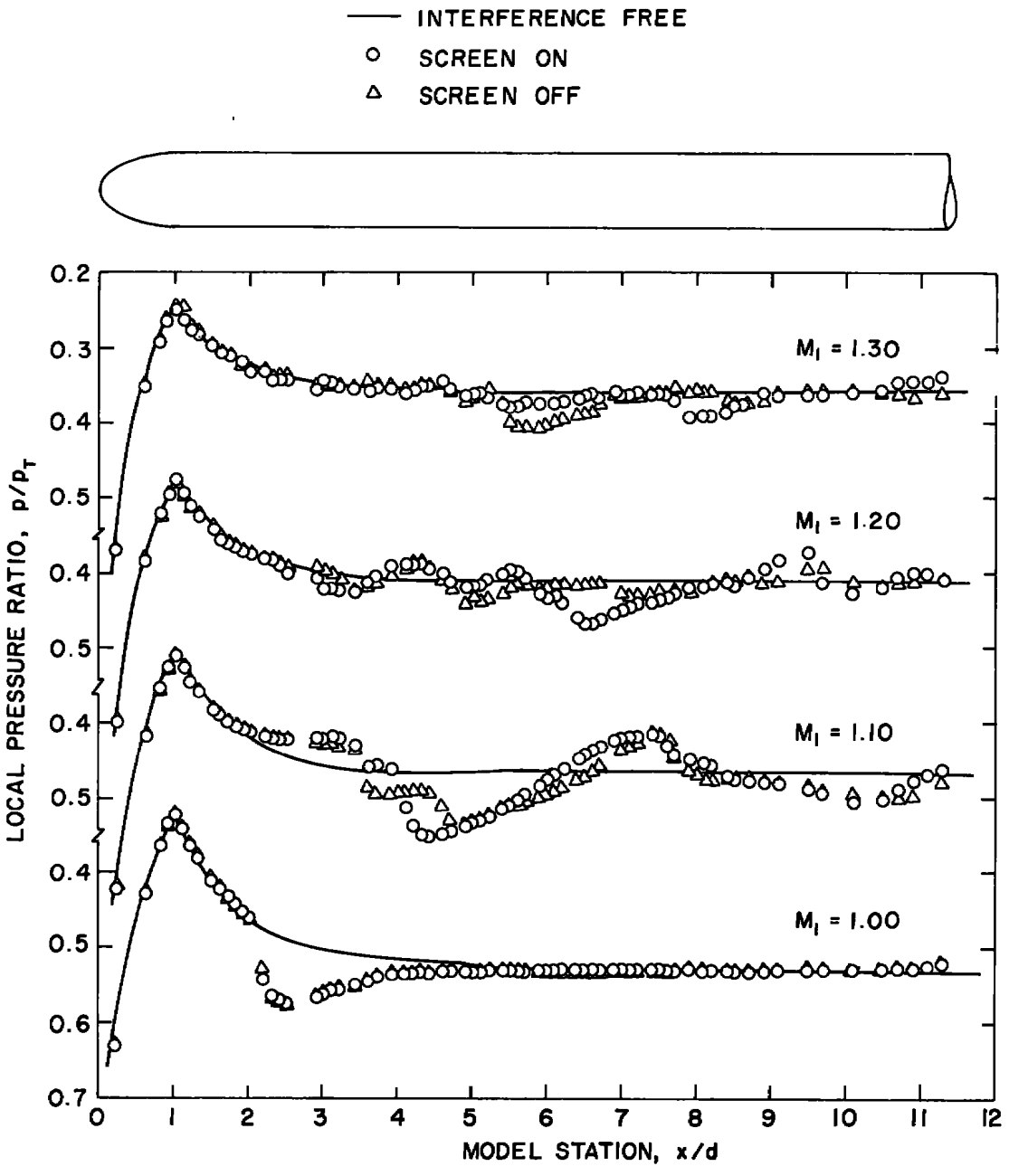

Figure 9. Pressure distribution on the ellipse-cylinder model, τ = 5 percent.

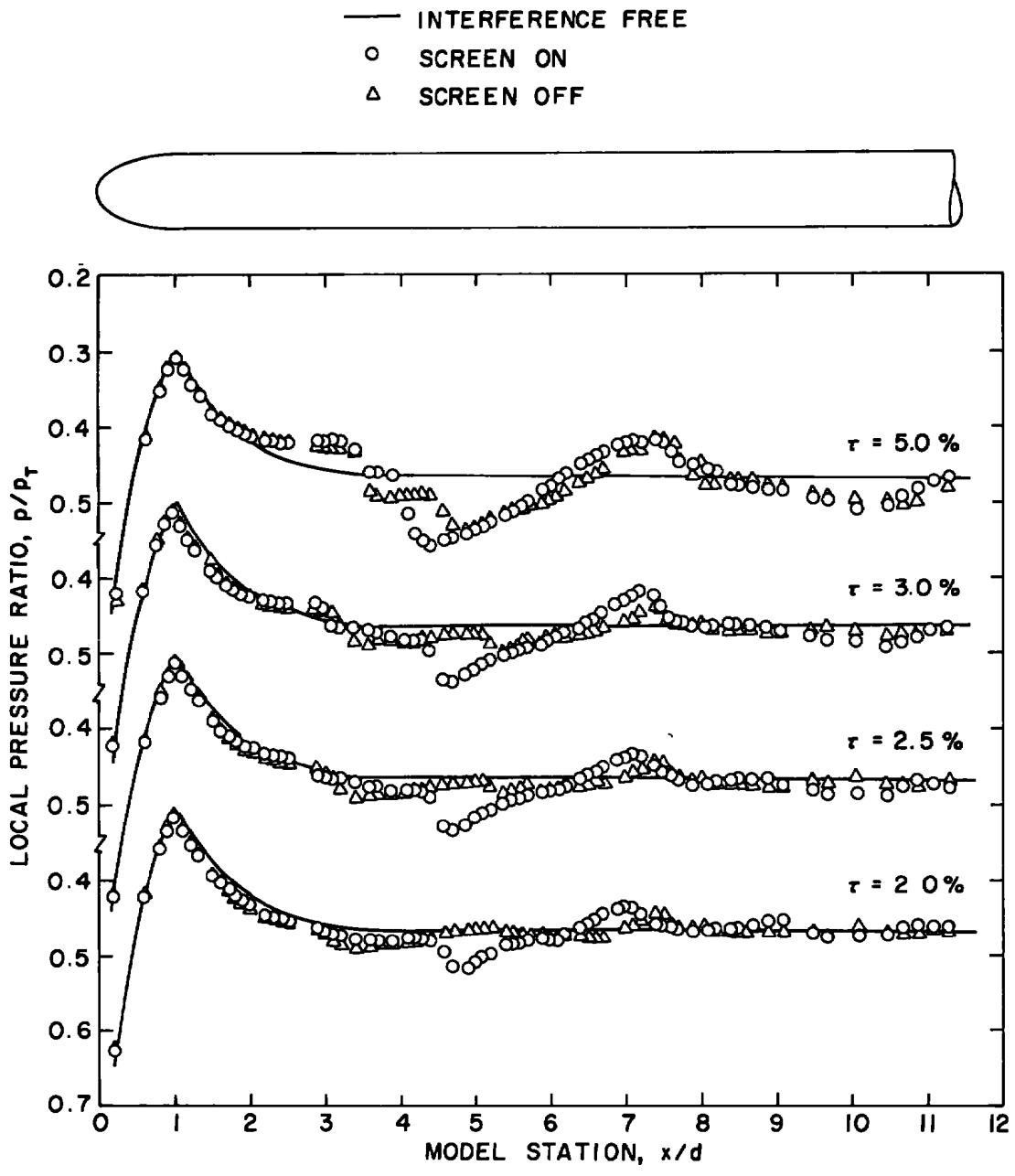

Figure 10. Pressure distribution on the ellipse-cylinder model for various porosities at M_1 = 1.10.

4.3 NOISE REDUCTION

The primary acoustic disturbance produced in perforated wall wind tunnel test sections is edgetones generated by the individual holes. At some Mach number, depending

on the wall geometry and test section dimensions, a resonant condition occurs. This resonant condition takes place in Tunnel 4T at about M = 0.8. The overall noise level is generally presented in terms of the fluctuating pressure coefficient, ΔC_P, defined as:

$$\Delta C_p = \frac{P_{rms}}{q_\infty} \times 100, \text{ percent}$$

where P_{rms} is the time-averaged, frequency-integrated fluctuating pressure measured by microphones. A ΔC_P level of 0.5 percent corresponds to the expected level of sound radiation from a turbulent boundary layer.

Noise data obtained with and without the screen overlay are presented in Fig. 11. The noise reduction with the screen overlay was as great as threefold in ΔC_P at the resonant condition.

4.4 EFFECTS ON TRANSITION

End-of-transition Reynolds number as measured with the transition cone is shown in Fig. 12. The porosity at each Mach number was individually selected for the two wall configurations, on the basis of the best wave cancellation properties. As shown in Fig. 12, there is a significant effect of the noise suppression on the transition Reynolds number. For the screen-on case, Re_T tends to remain at a constant value with Mach number and unit Reynolds number, as does the noise level. Note that, comparing Figs. 11 and 12, there is a definite inverse trend of transition Reynolds number with noise level for the screen-off wall. The results shown in Fig. 12 may be affected at supersonic Mach numbers by the disturbances from the screen installation, as discussed in Section 4.1. Detailed information concerning the relationship between noise level and transition Reynolds number is presented in Ref. 4.

4.5 LIFTING MODEL RESULTS

Wing surface pressure distributions at Mach number 0.6 are shown in Figs. 13 and 14. Results with the standard 4T wall configuration (screen off) are presented in Fig. 13 to illustrate the insensitivity of the pressure distribution to Reynolds number at Mach number 0.6. A comparison of the screen-on and screen-off wall configuration data for the chord Reynolds number range from 0.71×10^6 to 2.3×10^6 is shown in Fig. 14. The data for the two wall configurations are in good agreement. The pressures in the leading-edge expansion region are extremely sensitive to small changes in angle of attack due to the magnitude of the pressure gradient, and the differences for the wall configurations as shown in Fig. 14 are within the normal data scatter. The lower surface pressure distribution is virtually the same for all three Reynolds numbers, so only one comparison is shown, to preserve clarity.

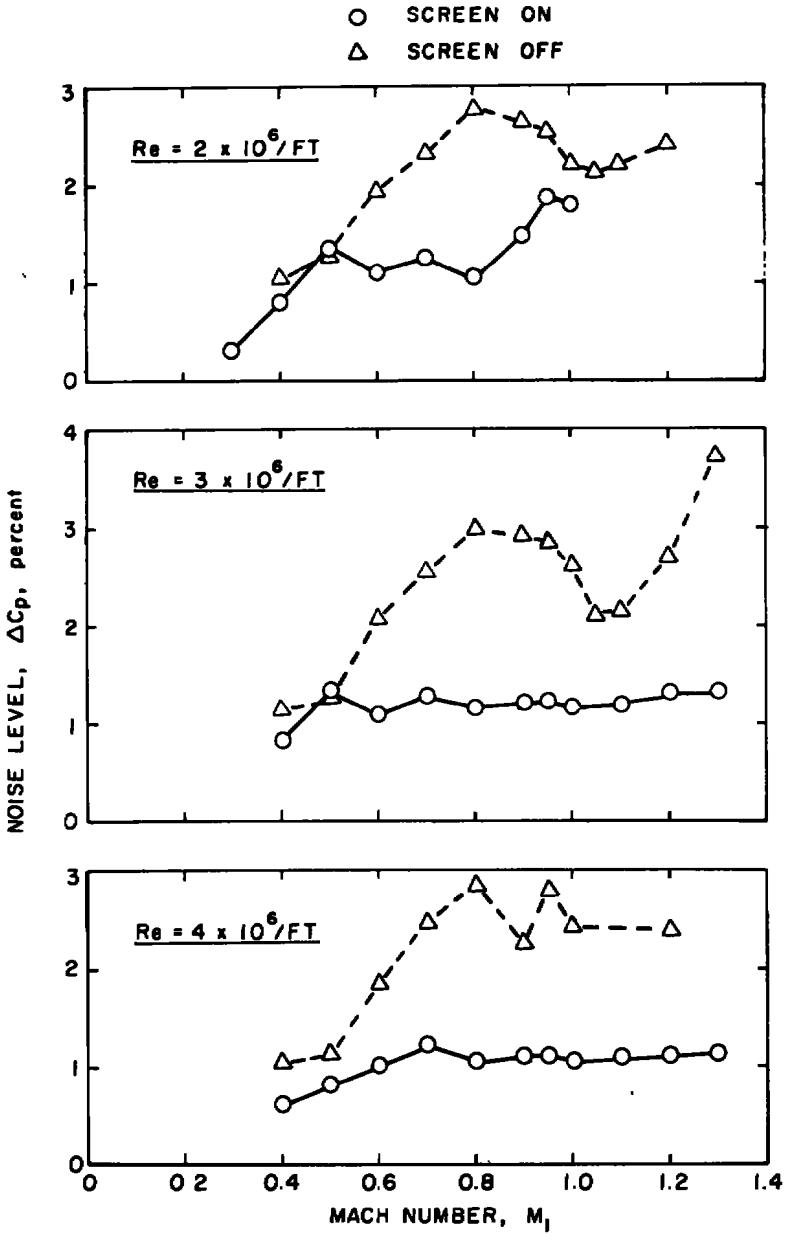

Figure 11. Comparison of the noise level with and without the wall screens.

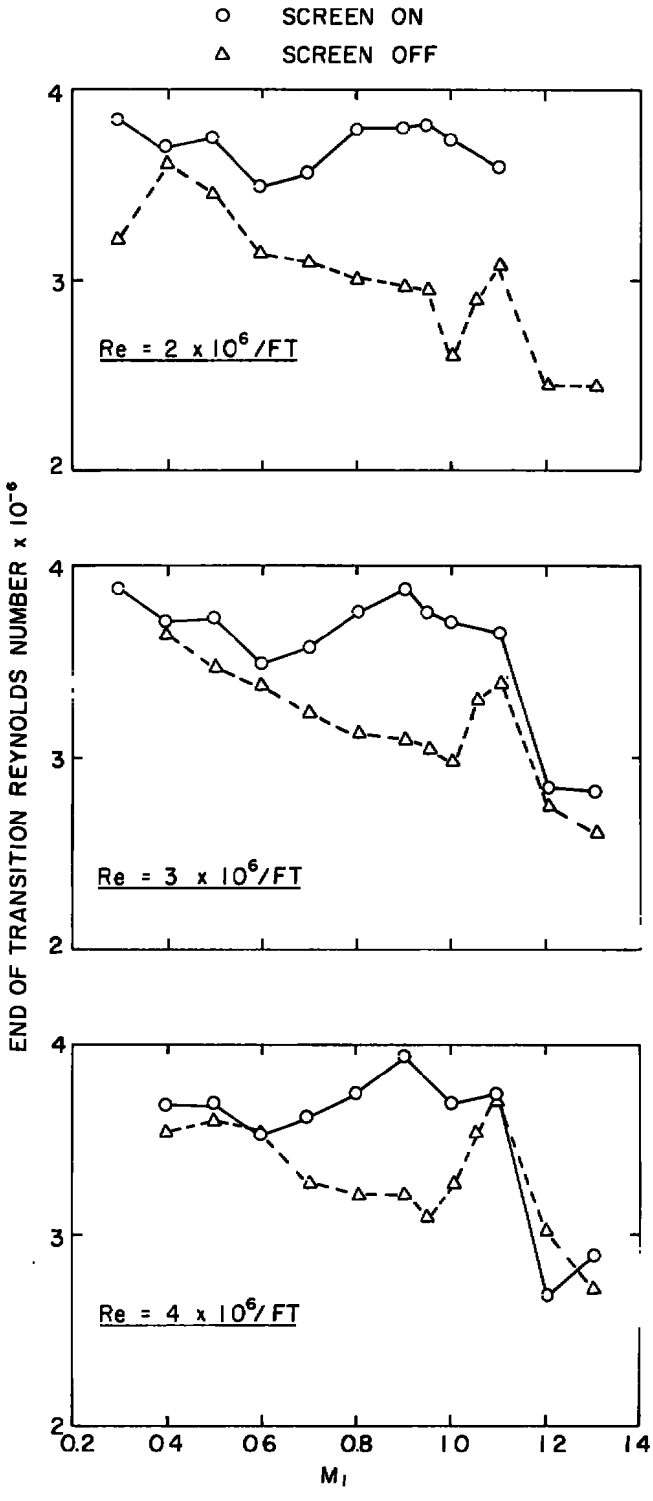

Figure 12. Comparison of end of transition Reynolds number with and without the wall screens.

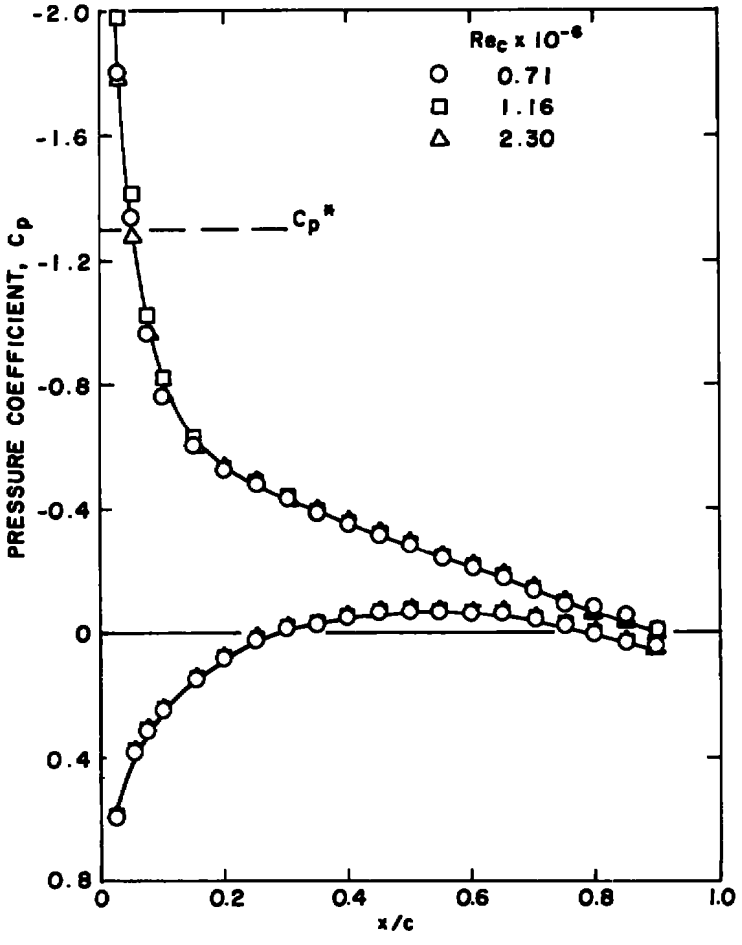

Figure 13. Wing surface pressure distribution variation with Reynolds number (screen off), M_1 = 0.60, α = 6 deg.

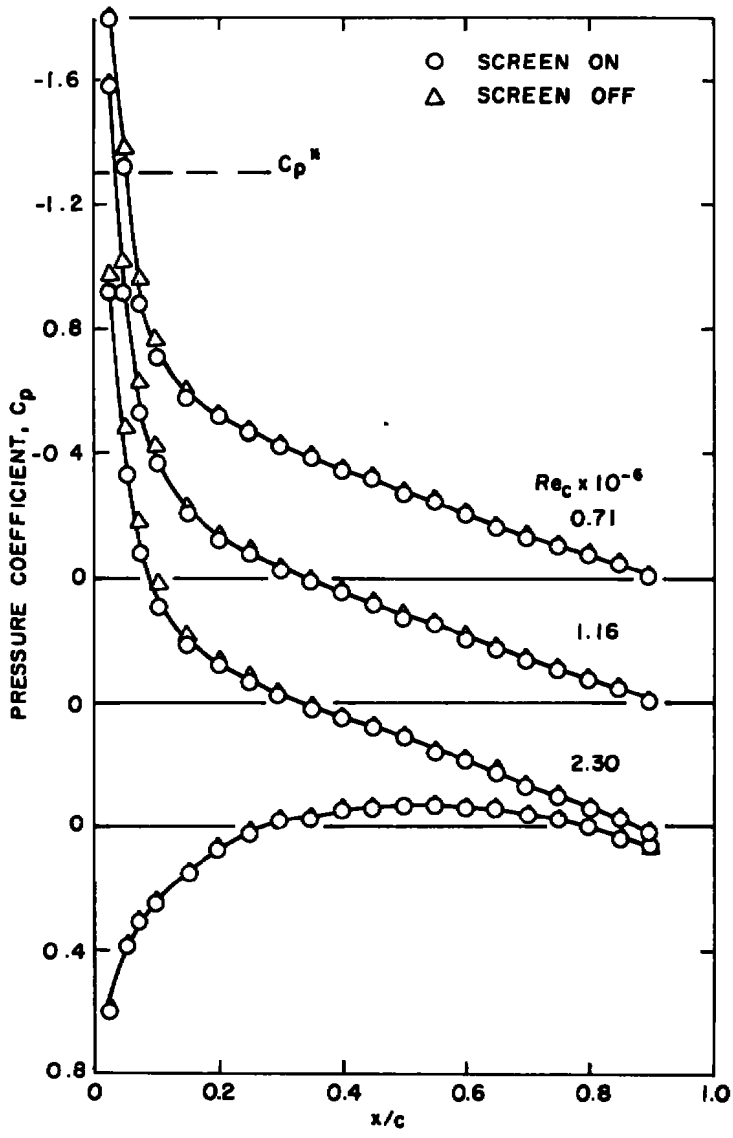

Figure 14. Comparison of the wing surface pressure distribution with and without the wall screens, M_1 = 0.60, α = 6 deg.

A comparison of the surface pressure distributions for various Reynolds numbers at M = 0.8 and α = 6 deg is shown in Fig. 15. The main shock moves rearward, and its strength increases with increasing Reynolds number. Comparison of the data with the screen on and off, Fig. 16, indicates a significant difference in the locations of the main shock at the highest Reynolds number. Again, the lower surface distribution is representative of that for all three Reynolds numbers. The shock displacement appears at both 4 and 6 deg angle of attack when a strong shock exists, as shown in Fig. 17. The forward displacement of the main shock occurs both with reduced Reynolds number (Fig. 15) and with reduced noise (Fig. 16).

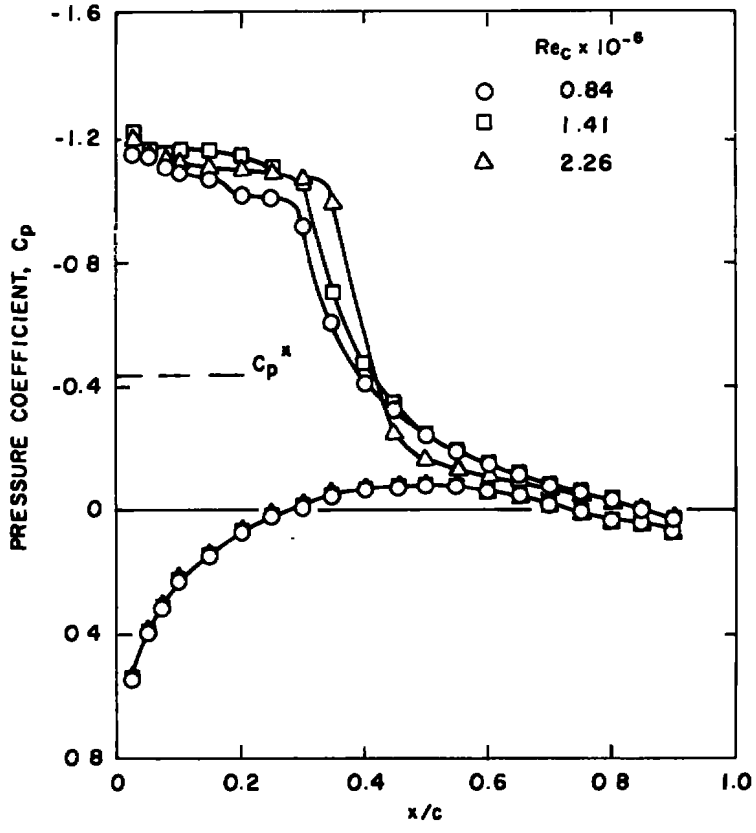

Figure 15. Wing surface pressure distribution variation with Reynolds number (screen off), M_1 = 0.80, α = 6 deg.

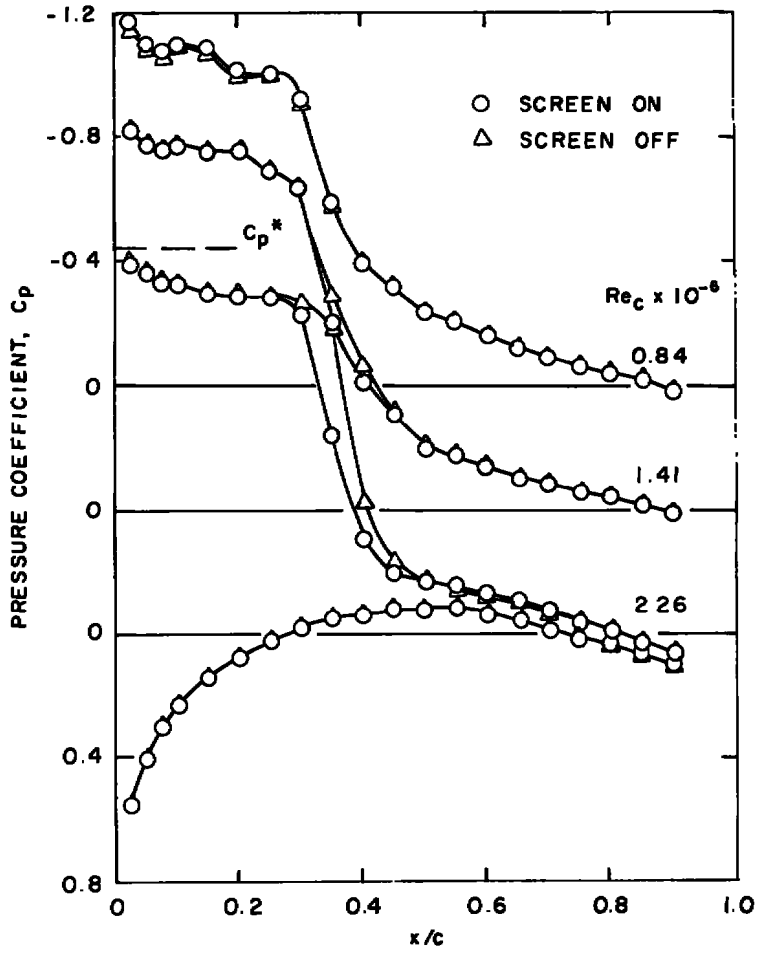

Figure 16. Comparison of the wing surface pressure distribution with and without the wall screens, M_1 = 0.80, α = 6 deg.

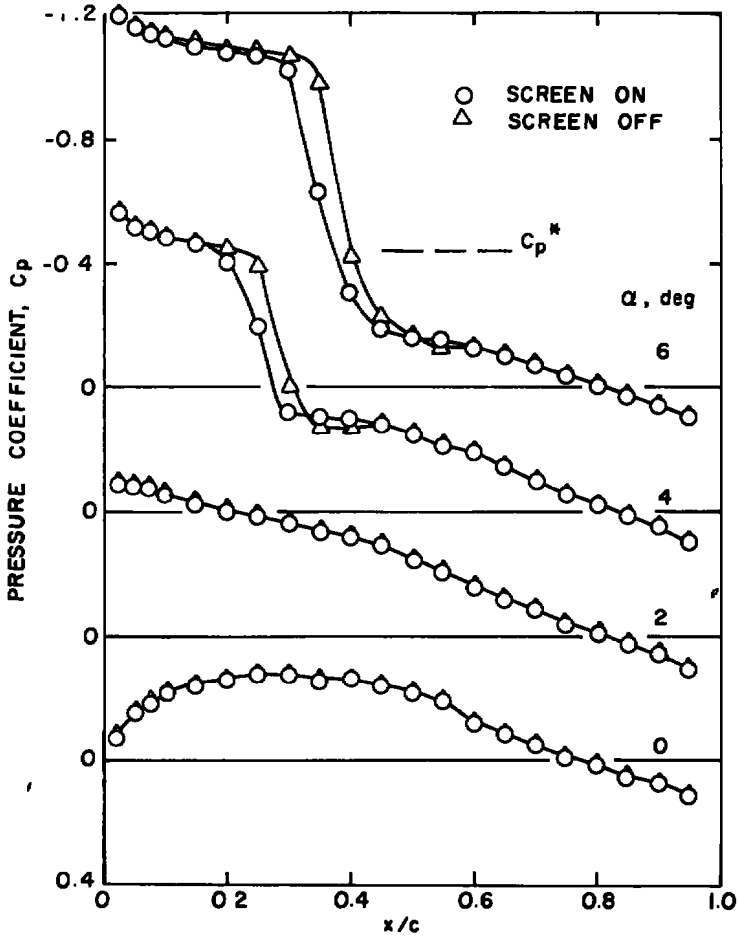

Figure 17. Variation of the upper surface pressure distribution with angle of attack, M_1 = 0.80, Re_c = 2.26 x 10^6.

Comparison of the upper surface pressure distributions for various Reynolds numbers at Mach number 0.90 is shown in Fig. 18. As Fig. 18a shows, for natural boundary-layer transition, as Reynolds number increases, the compression occurs over a shorter distance along the chord and the main shock is displaced forward. A separation bubble appears aft of the shock for a chord Reynolds number of 3.1 x 10^6, as evidenced by the inflection of the pressure distribution, and the bubble increases in size toward the trailing edge for a chord Reynolds number of 3.7 x 10^6. Detailed descriptions of this type of phenomenon on airfoils are attempted in Refs. 10, 11, and 12. Note that the effects of Reynolds number illustrated in Fig. 18a can be suppressed by fixing transition at the 5-percent chord location, as shown in Fig. 18b. The pressure distribution for all three Reynolds numbers is in good agreement. Note also that the shock is yet farther forward and the separation bubble aft of the shock is larger for the fixed transition cases

than for the highest chord Reynolds number with natural transition. The data in Fig. 18, then, imply that with increasing Reynolds number, as the boundary-layer transition moves forward on the surface, the recompression becomes a strong normal shock and a separation bubble appears aft of the shock and spreads toward the trailing edge. The main shock position also moves forward, probably as a result of the rearward separation.

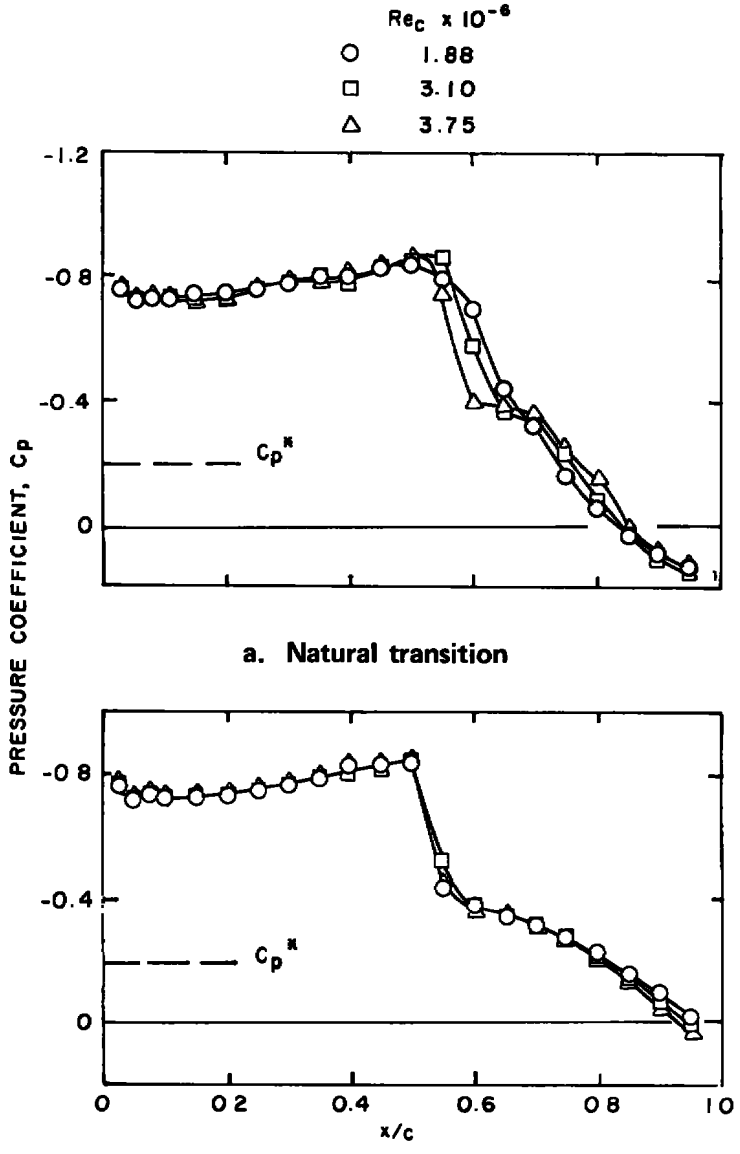

Figure 18. Wing surface pressure distribution variation with Reynolds number (screen off), M_1 = 0.90, α = 5.55 deg.

A comparison of the pressure distributions for the screen-on and screen-off walls at Mach number 0.9 and various Reynolds numbers is shown in Fig. 19. The lower surface distribution is representative of all the Reynolds numbers shown. A significant difference occurs at a chord Reynolds number of 2.93 x 10^6. The shock for the screen-off wall configuration is displaced upstream, and there is an extended separation bubble. There is little or no separation aft of the shock for the screen-on wall. The upper surface pressure distribution is shown in Fig. 20 for the angle-of-attack range from 0 to 6 deg and a chord Reynolds number of 2.93 x 10^6. The effect of the noise reduction (screen on) exhibited in Figs. 19 and 20 in each case is similar to that of reducing Reynolds number, as shown in Fig. 18.

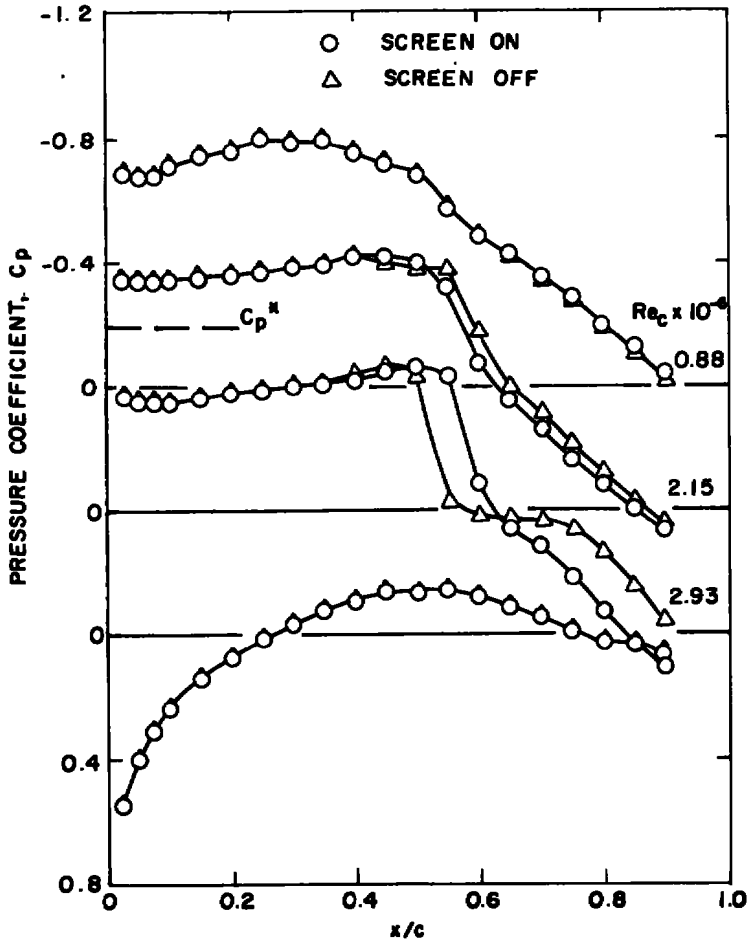

Figure 19. Comparison of the wing surface pressure distribution with and without the wall screens, M_1 = 0.90, α = 6 deg.

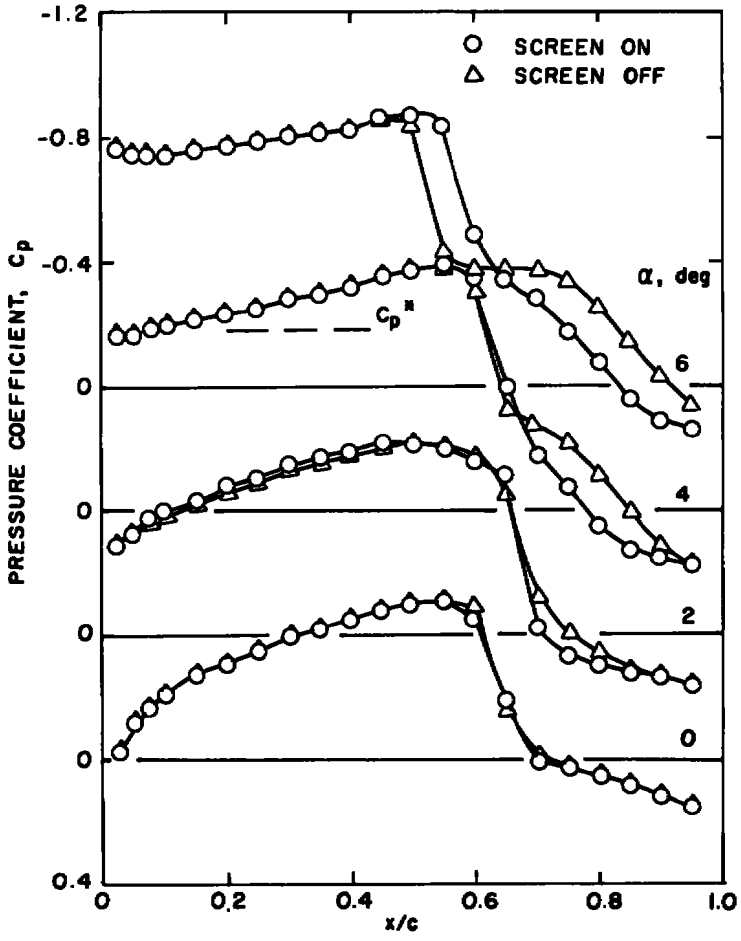

Figure 20. Variation of the upper surface pressure distribution with angle of attack, M_1 = 0.90, Re_c = 2.93 x 10^6.

In Section 4.2 the screen-on configuration was shown to cause a small change in the wall crossflow characteristic. Therefore, classical wall interference effects (the presence of the wall itself as opposed to unconfined flow) cannot be ignored as the cause of the difference between the pressure distribution for the two wall configurations. The effect of reducing the wall porosity (τ) from 5 to 2 percent is illustrated in Fig. 21. The effect of wall porosity adjustment for each Mach number is simply a displacement of the shock location, the shock for τ = 2 percent being displaced aft of that for τ = 5 percent. This is consistent with wall interferenc studies (Ref. 13, for example) which show aft shock displacement resulting from reducing the porosity of the ventilated walls. Fixing transition does not alter the basic character of the wall interference effects as seen in Fig. 21b. The effect of fixing transition is shown for Mach number 0.8 in Fig. 22 and for

Mach number 0.9 in Fig. 23 at the Reynolds numbers where the biggest difference between the screen-on and screen-off configurations occurred. The relative difference between the distribution for the two configurations remains essentially unchanged at Mach number 0.8. However, at Mach number 0.9, fixing transition brings the distribution for the wall configurations into agreement as it did for the Reynolds number variation in Fig. 18. Note also that the shock displacement between the two wall configurations at

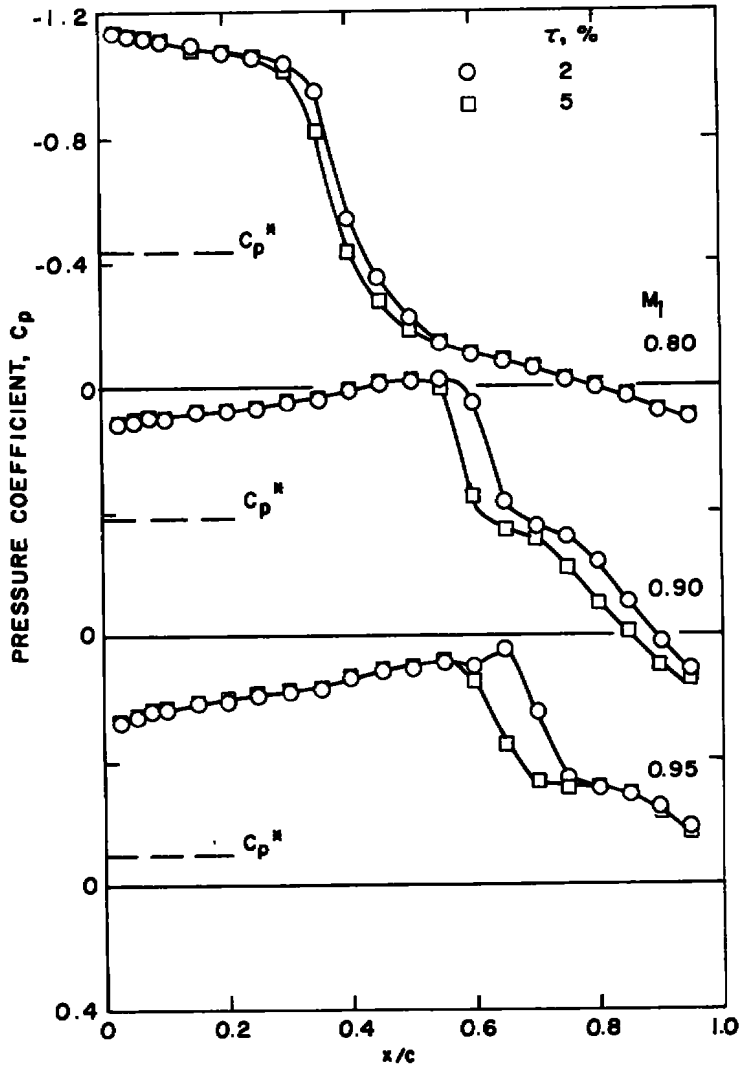

a. Natural transition

Figure 21. Wing upper surface pressure distribution variation with porosity (screen off), $Re_c = 2 \times 10^6$.

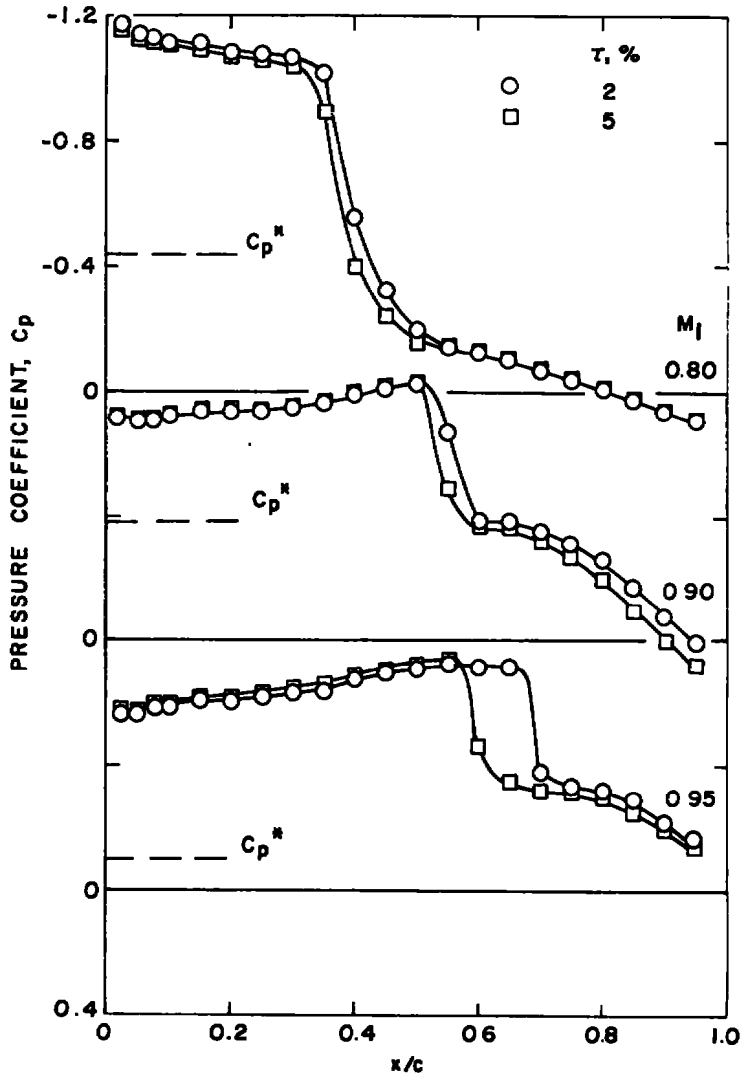

b. Fixed transition
Figure 21. Concluded.

Mach number 0.9 is opposite that resulting from wall interference effects; i.e., the shock location for the screen-on (more open) wall is aft of that for the screen-off wall. The cause of the difference in the pressure distribution at Mach number 0.80 cannot be identified as noise or wall interference effects. However, at Mach number 0.90, the disagreement can be attributed to noise effects.

At Mach number 0.95, the differences between the pressure distributions for the wall configurations with and without screens are less pronounced, but are of similar form to those for Mach number 0.90, as can be seen in Figs. 24 and 25. The comparison of the

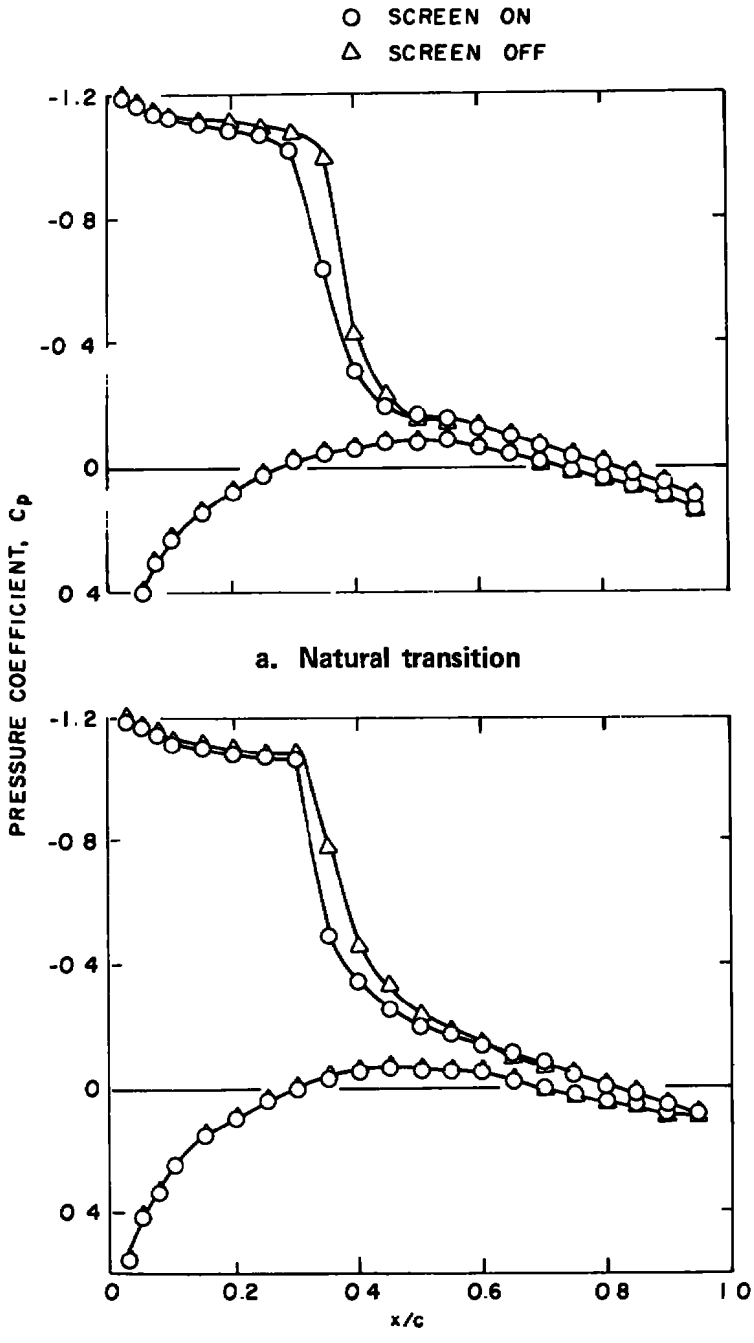

a. Natural transition

b. Fixed transition

Figure 22. Effect of fixing transition on the wing surface pressure distribution at M_1 = 0.80, Re_c = 2.26 x 10^6, α = 6 deg.

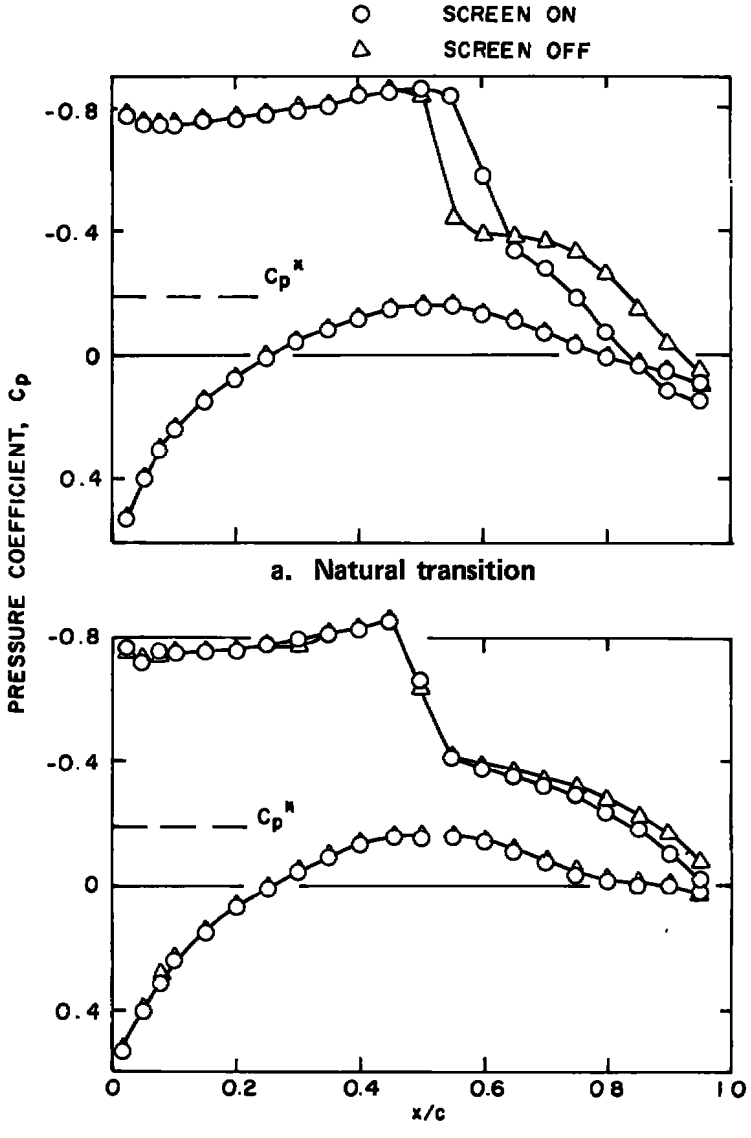

Figure 23. Effect of fixing transition on the wing surface pressure distribution at M_1 = 0.90, Re_c = 2.93 x 10^6, α = 6 deg.

pressure distributions at various Reynolds numbers for the screen-off wall is presented in Fig. 24. The upper surface pressure distribution for the angle-of-attack range from 0 to 6 deg is shown in Fig. 25. Again, when a difference exists, the effect of reducing the noise level with the screen is similar, but not equivalent, to that of reducing the Reynolds number.

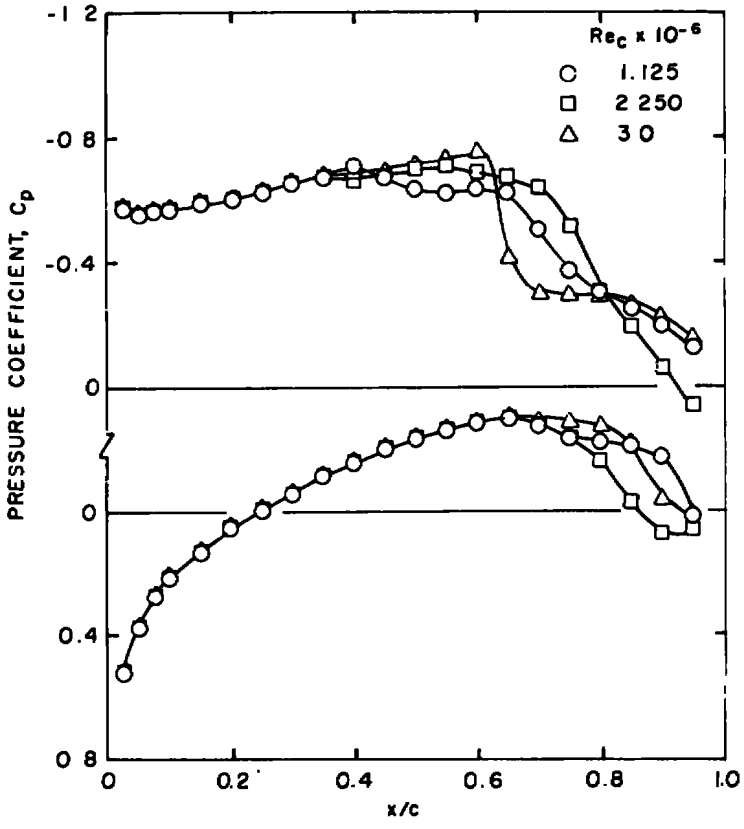

Figure 24. Wing surface pressure distribution variation with Reynolds number, M_1 = 0.95, α = 5.45 deg.

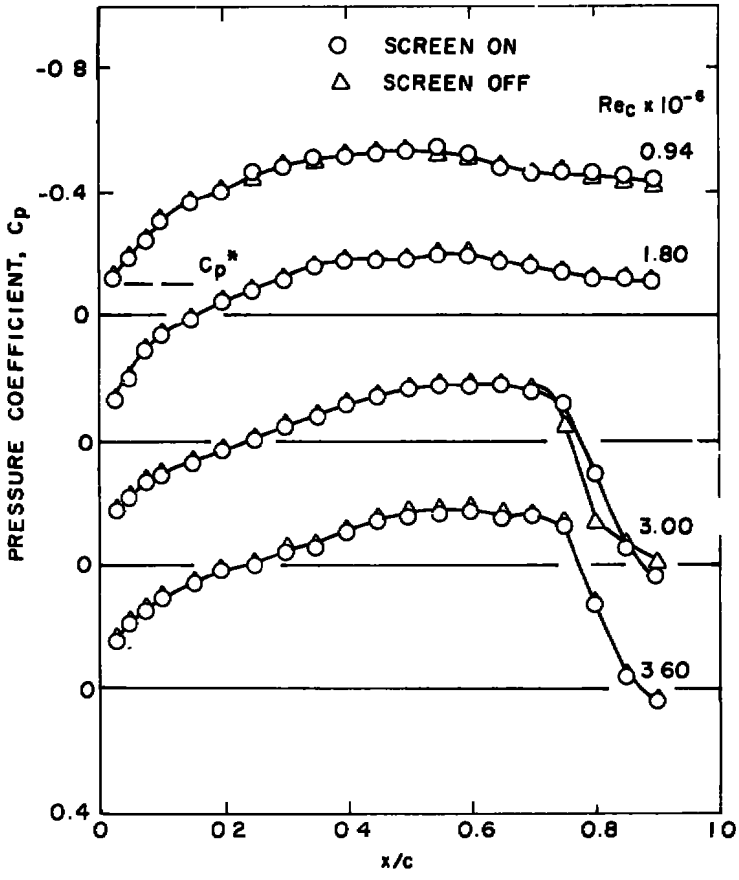

a. $\alpha = 0$

Figure 25. Comparison of the wing upper surface pressure distribution with and without the wall screens, $M_1 = 0.95$.

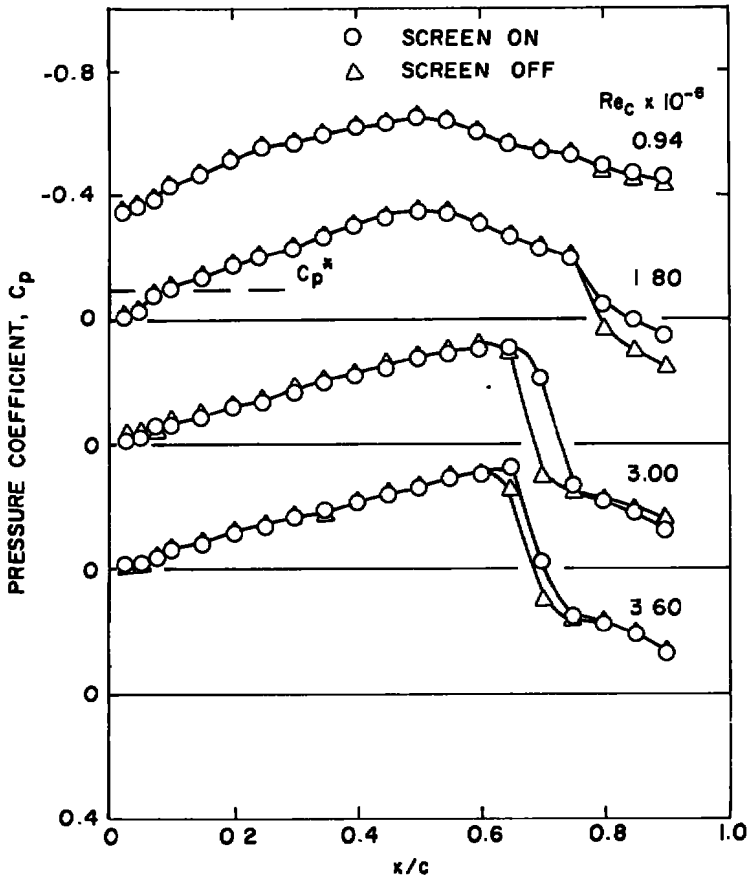

b. α = 4 deg

Figure 25. Continued.

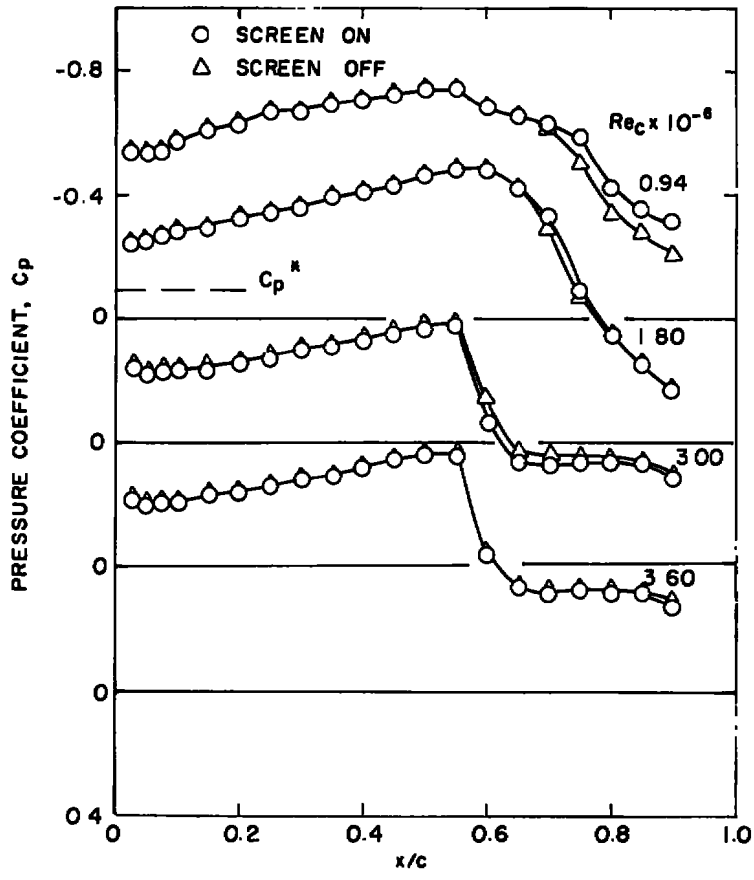

c. α = 6 deg

Figure 25. Concluded.

5.0 CONCLUDING REMARKS

It has been demonstrated that use of a screen overlay on the test section wall is a viable method of reducing the wall noise level. Although the present screen installation generally resulted in increased longitudinal flow nonuniformity, it is expected that a permanent installation would yield good quality airflow comparable to that obtainable without screens. The screen overlay adversely affected the wave cancellation properties of the variable porosity wall.

The noise level in the test section was reduced threefold in terms of ΔC_P at the resonant conditions. The ΔC_P value for the screen overlay wall was generally constant with Reynolds number and Mach number. Correspondingly, the transition Reynolds number increased with reduced noise and also became generally invariant with Mach number and Reynolds number; this behavior strongly suggests a dependency of transition Reynolds number on the acoustic environment.

Effects of the acoustic energy were also observed on the wing surface pressure distribution in localized ranges of Reynolds number, Mach number, and angle of attack, predominantly at Mach number 0.90. The effect of reducing the noise level by suppressing the edgetone generation was similar, but not necessarily equivalent, to a decrease in Reynolds number. This effect apparently is visible only when the boundary layer is undergoing transition either near the shock location or at relatively small distances upstream of the shock.

REFERENCES

1. Dougherty, N. S., Jr., Anderson, C. F., and Parker, R. L. "An Experimental Investigation of Techniques to Suppress Edgetones from Perforated Wind Tunnel Walls." AEDC-TR-75-88 (ADA013728), August 1975.

2. Schutzenhofer, L. A. and Howard, P. W. "Suppression of Background Noise in a Transonic Wind-Tunnel Test Section." AIAA Journal, Vol. 13, No. 11, November 1975, pp. 1467-1471.

3. Hartley, M. S. and Jacocks, J. L. "Static Pressure Distribution on Various Bodies of Revolution at Mach Numbers from 0.60 to 1.60." AEDC-TR-68-37 (AD828571), March 1968.

4. Dougherty, N. S., Jr. and Steinle, F. W., Jr. "Transition Reynolds Number Comparisons in Several Major Transonic Tunnels." AIAA Paper 74-627, July 1974.

5. Gunn, J. A. "Calibration of the AEDC-PWT Aerodynamic Wind Tunnel (4T) Using Diffuser Flap Plenum Suction." AEDC-TR-70-74 (AD867975), April 1970.

6. Jacocks, J. L. and Hartley, M. S. "Calibration of the AEDC-PWT 4-Ft Transonic Tunnel with Modified Walls." AEDC-TR-69-134 (AD853841), June 1969.

7. Reed, T. D., Pope, T. C., and Cooksey, J. M. "Calibration of Transonic and Supersonic Wind Tunnels." NASA CR 2920 (Vought Corporation), November 1977.

8. Jacocks, J. L. "Determination of Optimum Operating Parameters for the AEDC-PWT 4-ft Transonic Tunnel with Variable Porosity Test Section Walls." AEDC-TR-69-164 (AD857045), August 1969.

9. Hsieh, T. "Unsteady Transonic Flow over Blunt and Pointed Bodies of Revolution." AIAA Paper 78-211, January 1978.

10. Pearcey, H. H. "Some Effects of Shock-Induced Separation of Turbulent Boundary Layers in Transonic Flow Past Aerofoils." R&M No. 3108, 1959.

11. Pearcey, H. H., Haines, A. B., and Osborne, J. "The Interaction Between Local Effects at the Shock and Rear Separation - A Source of Significant Scale Effects in Wind-Tunnel Tests on Aerofoils and Wings." AGARD CP No. 35, "Transonic Aerodynamics," September 1968, pp. 11-1 to 11-23. Presented at the AGARD Specialists Meeting on Transonic Aerodynamics, September 1968.

12. Inger, G. R. "On Transonic Shock Wave-Boundary Layer Interaction Flow Patterns." VPI-Aero-018, August 1974.

13. Binion, T. W., Jr. "An Investigation of Three-Dimensional Wall Interference in a Variable Porosity Transonic Wind Tunnel." AEDC-TR-74-76 (AD787658), October 1974.

14. Jacocks, J. L. "Aerodynamic Characteristics of Perforated Walls for Transonic Wind Tunnels." AEDC-TR-77-61, June 1977.

15. Parker, R. L. "Flow Generation Properties of Five Transonic Wind Tunnel Test Section Wall Configurations." AEDC-TR-75-73 (ADA014260), August 1975.

APPENDIX A
PLENUM-STREAM CALIBRATION

For perforated wall wind tunnels, it is generally accepted that the relationship between plenum pressure and test section pressure is independent of model size or shape. This assumption permits the setting and determination of test section Mach number from measurements of the tunnel stagnation and plenum pressures.

A plenum Mach number (M_c) is defined on the basis of an isentropic expansion from stagnation to plenum pressure and a relationship formed to express the difference (DM) between the average test section Mach number (M_1) and M_c as a function of the pertinent independent variables. For the screen installation, the primary independent parameters were determined to be M_c and wall porosity (τ), and a least-square surface fit was constructed in the form of

$$DM = M_1 - M_c = \sum_{i=0}^{5} \sum_{j=0}^{5} C_{ij} M_c^i \tau^j, \quad i + j \leq 5$$

where the constants are given in Table 1. A comparison of the data and the surface fit is presented in Fig. A-1. These results are significantly different from the plenum-stream calibration of the basic tunnel (screens off). Some calibration data were obtained at stagnation pressure levels other than 2,000 psfa that indicated the plenum-stream calibration with screens was insensitive to Reynolds number within measurement accuracy.

Reference 14 argues that the plenum-stream calibration concept is incorrect and should be reexamined. To address this problem, several static pressure taps were installed in the test section walls, as mentioned previously, and data were obtained during each phase of testing. Somewhat surprisingly, the screen overlay did not significantly affect the accuracy of the wall pressure measurements. During the tunnel calibration phase, the wall static pressures were in agreement with the centerline measurements, screens on and off. However, with either of the one-percent-blockage models and the screens installed, a consistent deviation was observed between the calibrated Mach number (M_1) and that indicated by the wall static pressure taps for subsonic Mach numbers and low wall porosity. Representative results are given in Fig. A-2 in the form of $M_1 - M_w$. An indication of the true Mach number (M_∞) with the cone-cylinder model installed can be obtained by comparing the cone static pressure distribution to the data of Ref. 3. These results are also given in Fig. A-2 ($M_1 - M_\infty$), where the screen-off data are reproduced from Ref. 8. Both the model pressure distribution and the wall pressure distribution indicate that the plenum-stream calibration is not valid at low wall porosities. Similar results are given in Ref. 15.

Comparison of the Mach number differences with the cone and wall pressures indicates that less error in Mach number would result through use of the wall static pressure to set Mach number rather than the plenum-stream calibration. However, this is not a satisfactory solution because the proper location of the wall static pressure is a function of Mach number. Further analysis is required before an alternative method of determining test section Mach number can be recommended. Use of the plenum-stream calibration introduces insignificant errors at moderate wall porosity with a model blockage of one percent or less.

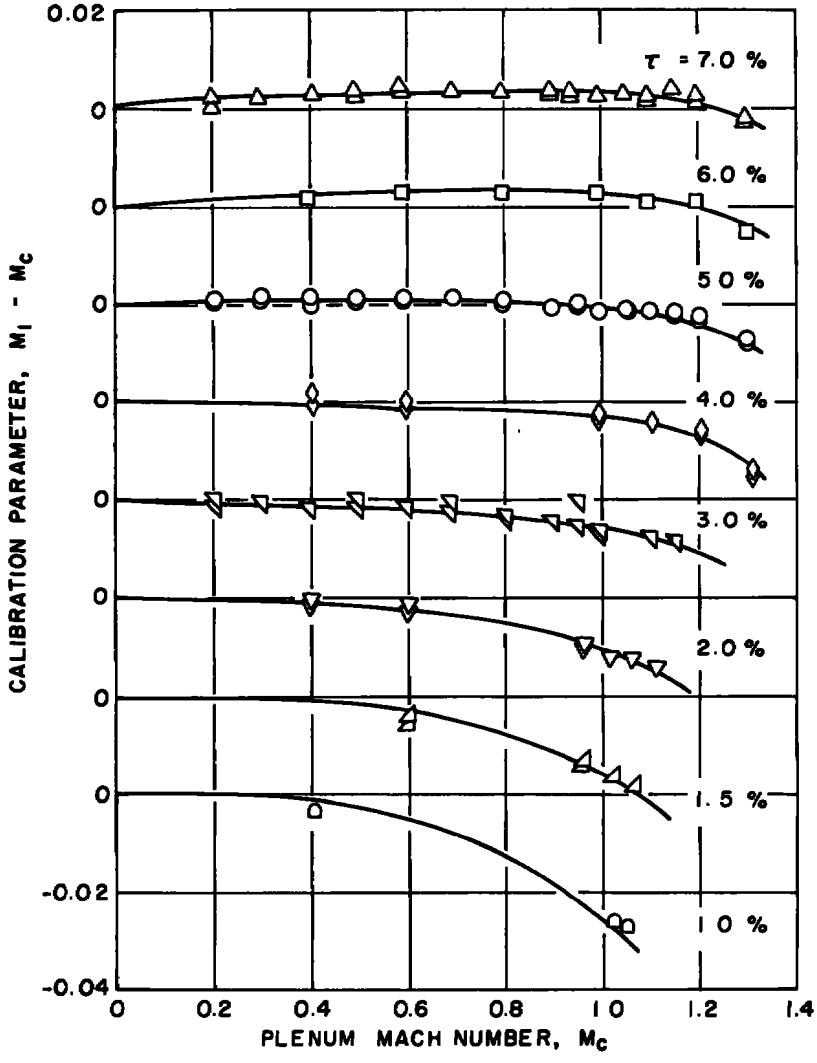

Figure A-1. Plenum-stream calibration.

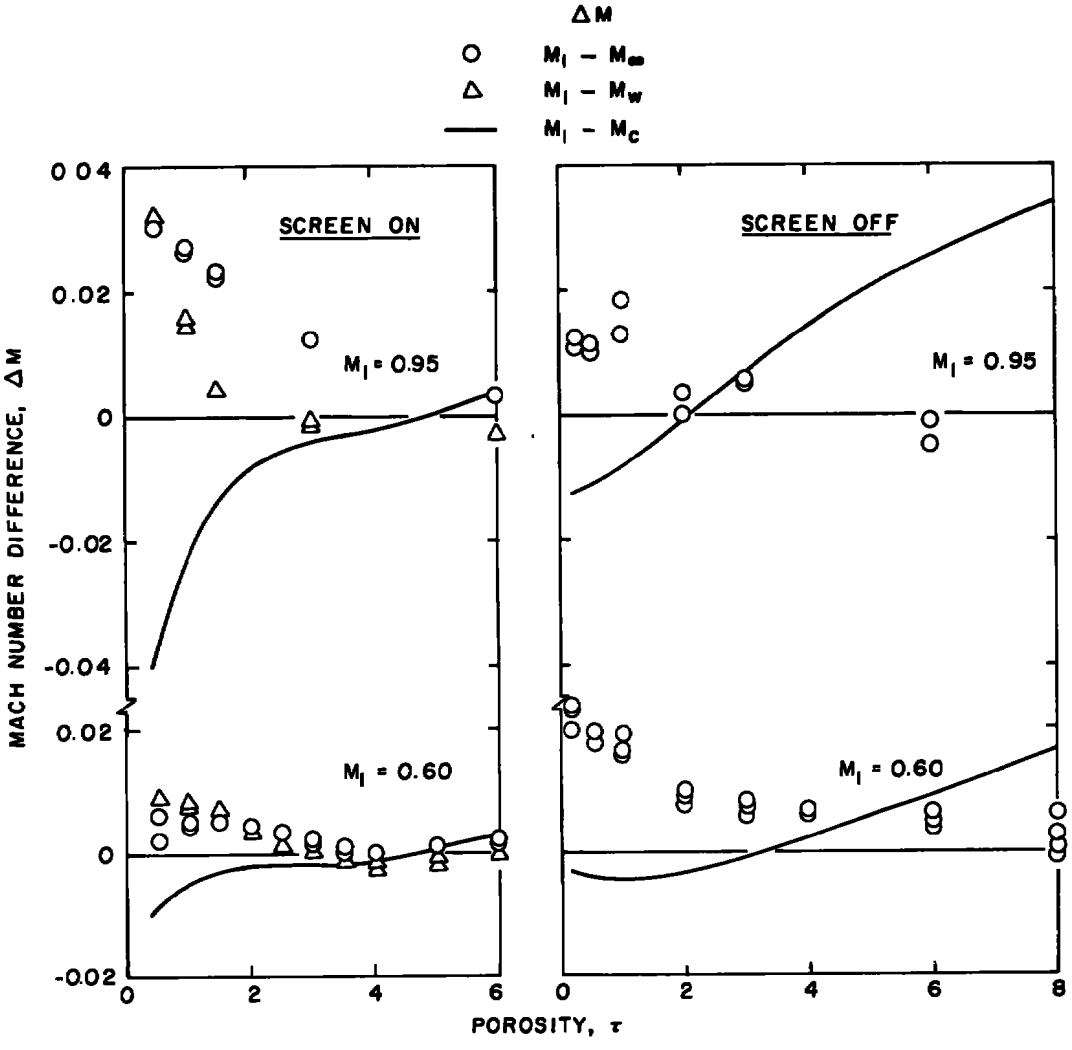

Figure A-2. Mach number errors introduced by using the plenum-stream calibration.

Table A-1. Plenum-Stream Calibration Constants

$$DM = \sum_{i=0}^{5} \sum_{j=0}^{5} C_{ij} M_c^i \tau^j, \quad i + j \leq 5$$

ij	C_{ij}
00	1.1352-03
10	1.0090-04
01	-1.6220-03
20	-9.4967-03
11	6.1341-03
02	1.7902-04
30	-1.0296-01
21	4.2736-02
12	-9.6376-03
03	3.0871-04
40	7.4659-02
31	1.2886-02
02	-1.2121-02
13	2.7487-03
04	-9.3615-05
50	-3.0468-02
41	-3.2343-04
32	-8.5806-04
23	9.1565-04
14	-2.1161-04
05	7.2052-06

Note: $1.1352\text{-}03 = 1.1352 \times 10^{-3}$

NOMENCLATURE

C_P	Pressure coefficient
C_P*	Pressure coefficient at sonic conditions
c	Wing chord, in.
DM	Tunnel calibration parameter, M_l - M_c
d	Model diameter, in.
M	Mach number
M_l	Average test section centerline Mach number
M_c	Equivalent plenum Mach number
M_w	Test section wall Mach number
M_∞	Free-stream Mach number
P	Static pressure, psfa
P_c	Plenum pressure, psfa
P_E	Diffuser exit pressure, psfa
P_{rms}	Root mean square of pressure fluctuations, psf
P_T	Stagnation pressure, psfa
q_∞	Free-stream dynamic pressure, psf
Re	Unit Reynolds number of free stream, 1/ft
Re_c	Reynolds number referenced to model chord
Re_T	Reynolds number referenced to the end of transition
x	Model station, in.
α	Gravimetric angle of attack, deg
α_i	Sting support angle, deg

$\Delta\alpha$ Sting deflection angle, deg

ΔC_P Fluctuating pressure coefficient, P_{rms}/q_∞, percent

λ Tunnel pressure ratio, P_T/P_E

σ Standard deviation

τ Wall porosity, percent-open area